of cardiac and renal sympathetic nerve activities. *Am J Physiol Heart Circ Physiol* 280: H1581–H1590, 2001.
16. **Kawada T, Yamamoto K, Kamiya A, Ariumi H, Michikami D, Shishido T, Sunagawa K, Sugimachi M.** Dynamic characteristics of carotid sinus pressure-nerve activity transduction in rabbits. *Jpn J Physiol* 55: 157–163, 2005.
17. **Kawada T, Yanagiya Y, Uemura K, Miyamoto T, Zheng C, Li M, Sugimachi M, Sunagawa K.** Input-size dependence of the baroreflex neural arc transfer characteristics. *Am J Physiol Heart Circ Physiol* 284: H404–H415, 2003.
18. **Kawada T, Sugimachi M, Sato T, Miyano H, Shishido T, Miyashita H, Yoshimura R, Takaki H, Alexander J Jr, Sunagawa K.** Closed-loop identification of carotid sinus baroreflex open-loop transfer characteristics. *Am J Physiol Heart Circ Physiol* 273: H1024–H1031, 1997.
19. **Lohmeier TE, Iliescu R, Dwyer TM, Irwin ED, Cates AW, Rossing MA.** Sustained suppression of sympathetic activity and arterial pressure during chronic activation of the carotid baroreflex. *Am J Physiol Heart Circ Physiol* 299: H402–H409, 2010.
20. **Marmarelis PZ, Marmarelis VZ.** The white noise method in system identification. In: *Analysis* of Physiological Systems. New York: Plenum, 131–180, 1978.
21. **Mills E, Bruckert JW.** Pressor mechanisms linked obligatorily to spontaneous hypertension in the rat. *Hypertension* 11: 427–432, 1988.
22. **Mizuno M, Kawada T, Kamiya A, Miyamoto T, Shimizu S, Shishido T, Smith SA, Sugimachi M.** Dynamic characteristics of heart rate control by the autonomic nervous system in rats. *Exp Physiol* 95: 919–925, 2010.
23. **Mohrman DE, Heller LJ.** *Cardiovascular Physiology* **(6th ed).** New York: McGraw Hill, 2006, p. 172–177, 2006.
24. **Nosaka S, Wang SC.** Carotid sinus baroreceptor functions in the spontaneously hypertensive rat. *Am J Physiol* 222: 1079–1084, 1972.
25. **Liu HK, Guild SJ, Ringwood JV, Barrett CJ, Leonard BL, Nguang SK, Navakatikyan MA, Malpas SC.** Dynamic baroreflex control of blood pressure: influence of the heart vs. peripheral resistance. *Am J Physiol Regul Integr Comp Physiol* 283: R533–R542, 2002.
26. **Osborn JW.** Pathogenesis of hypertension in the sinoaortic-denervated spontaneously hypertensive rat. *Hypertension* 18: 475–482, 1991.
27. **Rho JH, Newman B, Alexander N.** Altered in vitro uptake of norepinephrine by cardiovascular tissues of spontaneously hypertensive rats. Part 1. In: *Mesenteric Artery Hypertension* 3: 704–709, 1981.
28. **Rho JH, Newman B, Alexander N.** Altered in vitro uptake of norepinephrine by cardiovascular tissues of spontaneously hypertensive rats. Part 2. Portal-mesenteric veins and atria. *Hypertension* 3: 710–717, 1981.
29. **Salgado HC, Barale AR, Castania JA, Machado BH, Chapleau MW, Fazan R Jr.** Baroreflex responses to electrical stimulation of aortic depressor nerve in conscious SHR. *Am J Physiol Heart Circ Physiol* 292: H593–H600, 2007.
30. **Sapru HN, Wang SC.** Modification of aortic baroreceptor resetting in the spontaneously hypertensive rat. *Am J Physiol* 230: 664–674, 1976.
31. **Sato T, Kawada T, Inagaki M, Shishido T, Sugimachi M, Sunagawa K.** Dynamics of sympathetic baroreflex control of arterial pressure in rats. *Am J Physiol Regul Integr Comp Physiol* 285: R262–R270, 2003.
32. **Sato T, Kawada T, Miyano H, Shishido T, Inagaki M, Yoshimura R, Tatewaki T, Sugimachi M, Alexander J Jr, Sunagawa K.** New simple methods for isolating baroreceptor regions of carotid sinus and aortic depressor nerves in rats. *Am J Physiol Heart Circ Physiol* 276: H326–H332, 1999.
33. **Sato T, Kawada T, Sugimachi M, Sunagawa K.** Bionic technology revitalizes native baroreflex function in rats with baroreflex failure. *Circulation* 106: 730–734, 2002.
34. **Shoukas AA, Callahan CA, Lash JM, Haase EB.** New technique to completely isolate carotid sinus baroreceptor regions in rats. *Am J Physiol Heart Circ Physiol* 260: H300–H303, 1991.
35. **Ursino M, Fiorenzi A, Belardinelli E.** The role of pressure pulsatility in the carotid baroreflex control: a computer simulation study. *Comput Biol Med* 26: 297–314, 1996.
36. **Yamaguchi I, Kopin IJ.** Blood pressure, plasma catecholamines, and sympathetic outflow in pithed SHR and WKY rats. *Am J Physiol Heart Circ Physiol* 238: H365–H372, 1980.

Autonomic Neuroscience: Basic and Clinical xxx (2010) xxx–xxx

Contents lists available at ScienceDirect

Autonomic Neuroscience: Basic and Clinical

journal homepage: www.elsevier.com/locate/autneu

Involvement of the mechanoreceptors in the sensory mechanisms of manual and electrical acupuncture

Hiromi Yamamoto [a,*], Toru Kawada [b], Atsunori Kamiya [b], Shunichi Miyazaki [a], Masaru Sugimachi [b]

[a] Division of Cardiology, Department of Medicine, Faculty of Medicine, Kinki University, Osaka, Japan
[b] Department of Cardiovascular Dynamics, National Cerebral and Cardiovascular Center Research Institute, Osaka, Japan

ARTICLE INFO

Article history:
Received 21 April 2010
Received in revised form 27 September 2010
Accepted 4 November 2010
Available online xxxx

Keywords:
Acupuncture
Arterial blood pressure
Heart rate
Mechanoreceptor
Gadolinium
Aortic depressor nerve

ABSTRACT

The modalities of acupuncture can be broadly classified into manual acupuncture (MA) and electroacupuncture (EA). Although MA has been reported to cause winding of tissue around the needle and subsequent activation of the sensory mechanoreceptors and nociceptors, the sensory mechanisms of acupuncture stimulation are not fully understood. To test the hypothesis that the involvement of the mechanoreceptors in the sensory mechanism is different in MA and EA, we examined the effects of a stretch-activated channel blocker gadolinium on the hemodynamic responses to hind limb MA and EA in anesthetized rats (n=9). Gadolinium significantly attenuated the MA-induced bradycardic response (−22±5 vs. −10±3 bpm, P<0.05) and tended to attenuate the MA-induced depressor response (−30±5 vs. −18±4 mm Hg, P=0.06). On the other hand, gadolinium significantly attenuated both the EA-induced bradycardic (−22±5 vs. −9±4 bpm, P<0.01) and depressor responses (−32±6 vs. −15±5 mm Hg, P<0.01). These results indicate that the mechanoreceptors are involved in the sensory mechanisms for both MA and EA.

1. Introduction

Acupuncture has been used to modulate autonomic nervous activity and cardiovascular function (Kimura and Sato, 1997; Lin et al., 2001). The modalities of acupuncture can be broadly classified into two categories: manual acupuncture (MA) and electroacupuncture (EA). MA and EA induce similar changes in the functional magnetic resonance imaging signal in the human brain (Napadow et al., 2005). Neural mechanisms involved in acupuncture have been the focus of investigations. The effects of EA are considered to be related to stimulation of finely myelinated (group III) and unmyelinated (group IV) fibers, which activate opioid receptors in the rostral ventrolateral medulla to inhibit sympathetic outflow (Chao et al., 1999). Depletion of group IV fibers by neonatal capsaicin treatment reduces the influence of EA on the pressor responses to mechanical stimulation of visceral organs (Tjen-A-Looi et al., 2005). The extensive network of tangential cutaneous axons, coupled with their communications with the large numbers of Merkel cells, might be considered a new division of the autonomic nervous system: the cutaneous intrinsic visceral afferent nervous system (Silberstein, 2009).

Although cardiovascular responses induced by acupuncture-like stimulation are known to be reflexes mediated via somatic afferent nerves, visceral afferent nerves and autonomic efferent nerves (Sato et al., 1994, 2002; Tjen-A-Looi et al., 2005; Uchida et al., 2007; Yamamoto et al., 2008; Silberstein, 2009), the sensory mechanisms of MA and EA that initiate afferent nerve discharge are not fully understood. Langevin et al. (2001) proposed that MA causes winding of tissues around the needle and subsequent activation of sensory mechanoreceptors and nociceptors, and also suggested that changes in extracellular milieu induced by MA are important factors for neuromodulation. Burnstock (2009) proposed that mechanical deformation of the skin leads to the release of ATP from keratinocytes, fibroblasts and other cells; then the sensory nerves are activated through purinergic receptors. Although EA may induce MA-like stimuli via electrical twitching of surrounding tissues, EA may also directly depolarize sensory axons and nerve terminals adjacent to the needle and induce reflex responses. If the direct depolarization is the major sensory mechanism of EA, inhibition of mechanoreceptors would not zsignificantly attenuate the effects of EA. On the other hand, if the mechanical stimulation plays a dominant role in the sensory mechanism of EA, inhibition of mechanoreceptors would significantly attenuate the effects of EA.

Among mechanoreceptors, mechanosensitive ion channels detect mechanical stimuli and transduce these stimuli into electrical signals in sensory neurons. Gadolinium chloride is widely used experimentally as an inhibitor of stretch-activated ion channels and physiological responses of tissues to mechanical stimulation (Adding et al., 2001). To test the hypothesis that the contribution of mechanoreceptors in the sensory mechanism differs in MA and EA, we examined the effects of gadolinium on the hemodynamic responses to MA and EA in anesthetized rats.

* Corresponding author. 377-2 Ohno-higashi, Osaka-sayama, Osaka 589-8511, Japan. Tel.: +81 72 366 0221; fax: +81 72 368 2378.
E-mail address: hiromi@med.kindai.ac.jp (H. Yamamoto).

1566-0702/$ – see front matter © 2010 Published by Elsevier B.V.
doi:10.1016/j.autneu.2010.11.004

2. Methods

2.1. Surgical preparation

Animal care was provided in strict accordance with the Guiding Principles for the Care and Use of Animals in the Field of Physiological Sciences approved by the Physiological Society of Japan. All protocols were reviewed and approved by the Animal Subject Committee at the National Cerebral and Cardiovascular Center. Male Wister Kyoto rats weighing from 310 to 460 g were anesthetized by an intraperitoneal injection of pentobarbital sodium (50 mg/kg) and ventilated mechanically via a tracheal tube with oxygen-enriched room air. The depth of anesthesia was maintained by continuous intravenous infusion of pentobarbital sodium (20–25 mg kg^{-1} h^{-1}) through a double lumen catheter inserted into the right external carotid vein. Ringer solution (6 mg kg^{-1} h^{-1}) was administered to maintain fluid balance. Arterial blood pressure (AP) was measured using a catheter inserted into the right common carotid artery. Heart rate (HR) was determined from AP using a cardiotachometer. Body temperature was maintained at approximately 38 °C using a heating pad.

2.2. MA and EA stimulations ($n=9$)

With the animal in the supine position, both hind limbs were lifted to obtain a better view of the lateral sides of the lower legs. An acupuncture needle with a diameter of 0.2 mm (CE0123, Seirin-Kasei, Japan) was inserted into a point below the knee joint just lateral to the tibia in the left or right leg. For MA stimulation, the acupuncture needle was inserted to a depth of 5–10 mm and manually twisted clockwise and counter-clockwise, and moved up and down at a frequency of 1–2 Hz for a duration of 120 s. Two to three MA trials were conducted with an intervening interval of more than 5 min within which AP and HR returned to the respective pre-stimulation values. For EA stimulation, another acupuncture needle was inserted into a point approximately 1 cm from the above-mentioned needle toward the ankle joint and used as the ground. EA was applied for 120 s using an isolator connected to an electrical stimulator (SEN 7203, Nihon Kohden, Japan). The pulse width and the stimulus current were set at 500 μs and 5 mA, respectively. The stimulation frequency was set at 10 Hz in six and at 20 Hz in three of the nine rats. The pulse duration was based on previous studies (Tjen-A-Looi et al., 2005; Yamamoto et al., 2008; Uchida et al., 2008). The amplitude and frequency were selected so that the magnitudes of reflex hemodynamic responses became comparable to those induced by MA before gadolinium administration. In each animal, two to three EA trials were conducted with an intervening interval of more than 5 min within which AP and HR returned to the respective pre-stimulation values.

Gadolinium chloride hexahydrate was dissolved in saline at a concentration of 20 mM (Nakamoto and Matsukawa, 2007). After performing MA and EA under control conditions, we administered the gadolinium solution intravenously (2 ml/kg). After 10 min, we repeated MA and EA. The acupuncture needle positions were kept unchanged between MA and EA trials as well as before and after the gadolinium administration.

In a supplemental protocol ($n=7$ additional rats), to examine the possibility that simple insertion of needles caused significant hemodynamic influences, an acupuncture needle (CE0123, Seirin-Kasei, Japan) was only inserted into a point below the knee joint just lateral to the tibia in the left or right leg and placed for a duration of 120 s. Needle was inserted to a depth of 5–10 mm.

2.3. Aortic depressor nerve stimulation ($n=6$)

Using a pair of platinum electrodes, we identified the aortic depressor nerve (ADN) running along the common carotid artery, based on the AP pulse-synchronous nerve activity monitored through a loud speaker. After a depressor response to brief electrical stimulation of the nerve was confirmed, the electrodes and the nerve were fixed and insulated by silicone glue (Kwik-Sil, World Precision Instruments, FL, USA). The nerve fibers caudal to the electrodes were then crushed by a tight ligature so that only the afferent fibers directed to the central nervous system were stimulated. In four of the six rats, the right ADN was stimulated. In the remaining two rats, the left ADN was stimulated because of failure to stimulate the right ADN properly. The ADN was stimulated for 120 s at a frequency of 50 Hz (pulse width: 2 ms, voltage: 2 V). ADN stimulation was repeated with an interval of 5 min until the AP and HR responses appeared to be reproducible under control conditions. We then administered the gadolinium solution intravenously (20 mM, 2 ml/kg). After 10 min, we repeated the ADN stimulation.

2.4. Data analysis

Data were digitized using a 16-bit analog-to-digital converter (Contec, Japan) and stored at 200 Hz on a laboratory computer system. First, AP and HR data were averaged every 10 s. Averaged time courses of AP and HR responses were then obtained from two to three trials of MA, EA or ADN stimulation in each animal. Next, the effects of MA, EA or ADN were examined using repeated-measures one-way analysis of variance (ANOVA) followed by Dunnett's test (Glantz, 2002). The baseline data point immediately before stimulation was treated as a single control point for the Dunnett's test. Finally, the maximum effect of MA, EA or ADN stimulation was quantified by the differences between the minimum and baseline values for AP and HR (ΔAP and ΔHR). The effects of gadolinium on ΔAP and ΔHR were examined by a paired-t test (Glantz, 2002). The differences were considered significant at $P<0.05$. Data are presented in mean ± SE values.

3. Results

Fig. 1 depicts the averaged time courses of AP and HR responses to MA ($n=9$ rats). MA gradually decreased AP and HR under control conditions. The minimum AP and HR were reached near the end of the MA stimulation period. After the cessation of MA, AP and HR gradually returned toward the respective baseline values. Intravenous gadolinium administration significantly decreased baseline AP from 138 ± 5 to 120 ± 5 mm Hg ($P<0.01$) but had no significant effect on baseline HR (379 ± 10 vs. 383 ± 7 bpm). Following gadolinium administration, although MA also decreased AP and HR significantly, ΔAP tended to be attenuated (−30 ± 5 vs. −18 ± 4 mm Hg; 68 ± 16% of the pre-gadolinium; $P=0.06$) and ΔHR was significantly attenuated (−22 ± 5 vs. −10 ± 3 bpm; 57 ± 23% of the pre-gadolinium; $P<0.05$) compared to control conditions.

Fig. 2 depicts the averaged time courses of AP and HR responses to EA ($n=9$ rats). Under control conditions, EA decreased AP and HR. Both responses reached almost a steady state at approximately 1 min of EA stimulation. AP and HR remained decreased during the rest of the EA stimulation period, and gradually returned toward the respective baseline values after the cessation of EA. Intravenous gadolinium administration significantly decreased baseline AP from 140 ± 5 to 123 ± 7 mm Hg ($P<0.01$) but did not affect baseline HR (385 ± 9 vs. 384 ± 7 bpm). Following gadolinium administration, although EA significantly decreased AP, the decrease in HR was only significant at 55 s of EA stimulation. ΔAP (−32 ± 6 vs. −15 ± 5 mm Hg; 38 ± 11% of the pre-gadolinium; $P<0.01$) and ΔHR (−22 ± 5 vs. −9 ± 4 bpm; 37 ± 14% of the pre-gadolinium; $P<0.01$) were attenuated significantly compared to control conditions.

In the supplemental protocol ($n=7$ rats), the insertion of an acupuncture needle alone did not significantly change AP (138 ± 9 vs. 138 ± 9 mm Hg) or HR (399 ± 20 vs. 400 ± 20 bpm).

Fig. 3 shows the averaged time courses of AP and HR responses to ADN stimulation ($n=6$ rats). ADN stimulation decreased AP and HR under control conditions. The minimum AP and HR were reached at 15 s of ADN stimulation. Both parameters remained decreased during the rest of the ADN stimulation period, and returned toward the respective

Please cite this article as: Yamamoto, H., et al., Involvement of the mechanoreceptors in the sensory mechanisms of manual and electrical acupuncture, Auton. Neurosci. (2010), doi:10.1016/j.autneu.2010.11.004

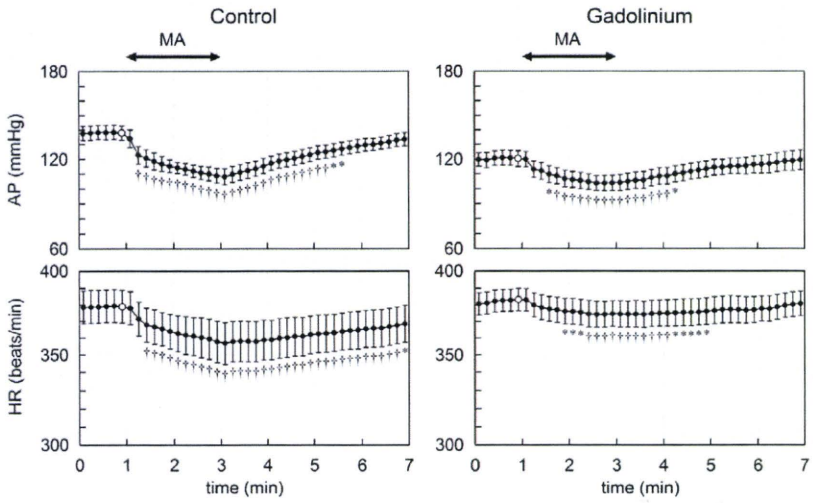

Fig. 1. Time courses of arterial pressure (AP) and heart rate (HR) responses induced by manual acupuncture (MA) averaged from 9 rats. MA gradually decreased AP and HR under control conditions (left) and after gadolinium administration (right). Gadolinium treatment tended to attenuate the AP response and significantly attenuated the HR response induced by MA, compared to control conditions. Data are mean ± SE values. *P<0.05 and †P<0.01 versus the control data point (open circle) immediately before the application of MA.

baseline values after the cessation of ADN stimulation. AP and HR appeared to recover more rapidly compared to those observed after MA and EA. Intravenous gadolinium administration significantly decreased baseline AP from 126 ± 4 to 118 ± 2 mm Hg (P<0.01) but had no significant effect on baseline HR (373 ± 13 vs. 369 ± 11 bpm). Following gadolinium administration, ADN stimulation significantly decreased AP and HR. Neither ΔAP (−43 ± 7 vs. −49 ± 3 mm Hg) nor ΔHR (−27 ± 8 vs. −34 ± 5 bpm) was attenuated compared to control conditions.

4. Discussion

We have shown that ion channels blocked by gadolinium are implicated in the hypotensive and bradycardic effects of acupuncture at the hind limb in rats, irrespective of technique.

4.1. Effects of gadolinium on AP and HR responses to MA and EA

Insertion of acupuncture needle alone did not change AP and HR significantly, indicating that continuous stimulation either by MA or EA was necessary to induce sustained AP and HR responses. Mechanoreceptors are thought to play an important role in the sensory mechanism of MA. Because gadolinium blocks mechanosensitive ion channels in sensory neurons (Cho et al., 2002), we hypothesized that intravenous administration of gadolinium would attenuate the AP and HR responses to MA. As expected, ΔAP tended to be attenuated after gadolinium administration (Fig. 1, top). However, since gadolinium also decreased baseline AP, it is uncertain whether the attenuation of ΔAP was mainly attributable to the inhibition of reflex response to MA or to the decreased baseline AP. On the other hand, gadolinium did not significantly affect baseline HR and

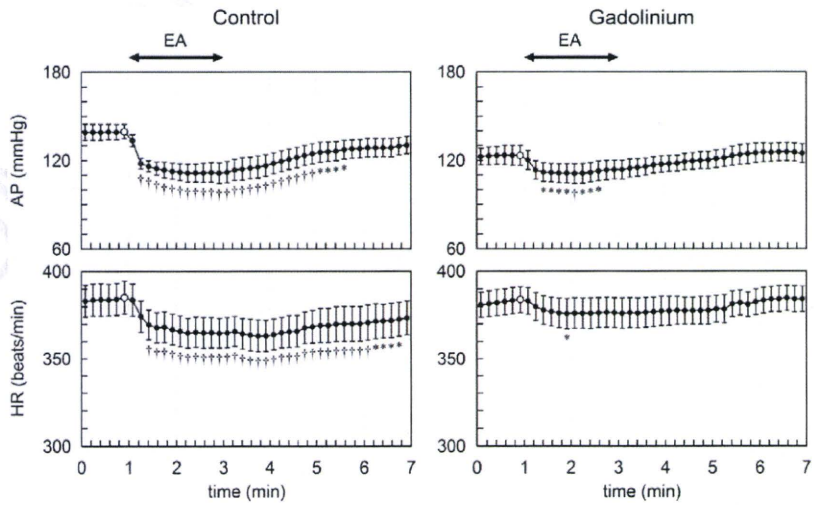

Fig. 2. Time courses of AP and HR responses induced by electroacupuncture (EA) averaged from 9 rats. EA gradually decreased AP and HR under control conditions (left) and after gadolinium administration (right). Gadolinium significantly attenuated both AP and HR responses induced by EA, compared to control conditions. Data are mean ± SE values. *P<0.05 and †P<0.01 versus the control data point (open circle) immediately before the application of EA.

Please cite this article as: Yamamoto, H., et al., Involvement of the mechanoreceptors in the sensory mechanisms of manual and electrical acupuncture, Auton. Neurosci. (2010), doi:10.1016/j.autneu.2010.11.004

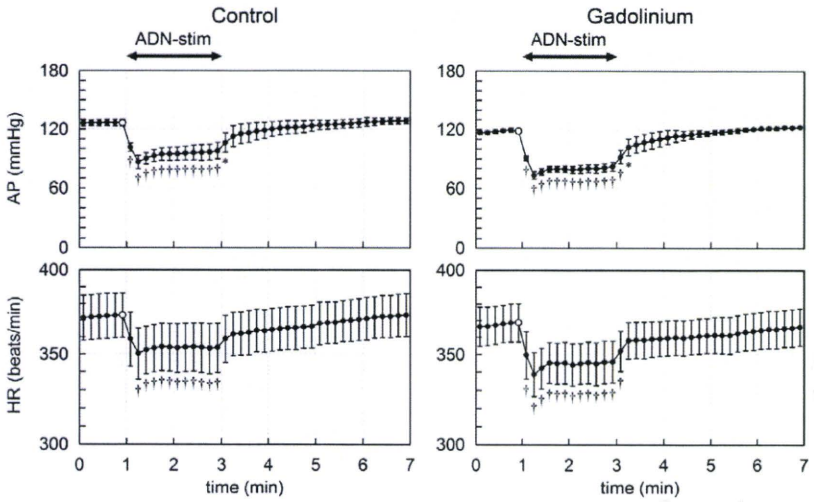

Fig. 3. Time courses of AP and HR responses induced by electrical stimulation of the aortic depressor nerve (ADN-stim) averaged from 6 rats. ADN-stim decreased AP and HR under control conditions (left) and after gadolinium administration (right). Gadolinium did not attenuate the AP and HR responses induced by ADN-stim, compared to control conditions. Data are mean ± SE values. $^{*}P<0.05$ and $^{\dagger}P<0.01$ versus the control data point (open circle) immediately before the application of ADN-stim.

significantly attenuated ΔHR induced by MA (Fig. 1, bottom). Judging from the HR response, it is conceivable that gadolinium inhibits the reflex hemodynamic responses to MA.

We assumed that direct depolarization of sensory axons and nerve terminals adjacent to the needle could be the major sensory mechanism of EA. In fact, direct electrical stimulation of muscle afferent fibers evokes a variety of cardiovascular responses similar to those induced by EA (Sato et al., 1981). If direct depolarization is the major sensory mechanism for EA, inhibition of mechanoreceptors would have no significant effect on EA, because the results of the ADN stimulation protocol indicates that the axonal conduction would not be blocked even after gadolinium administration once the afferent nerve is discharged (Fig. 3). Contrary to this assumption, gadolinium significantly attenuated ΔAP and ΔHR induced by EA (Fig. 2), suggesting that the mechanoreceptors play an important role in the sensory mechanism of EA, as in the case of MA. EA probably causes electrical twitching of surrounding tissues and exerts MA-like stimulation through the mechanoreceptors.

Despite the significant contribution of mechanoreceptors to the sensory mechanisms of both MA and EA, the fact that the hemodynamic responses to MA and EA were not entirely abrogated after gadolinium administration indicates the presence of sensory mechanisms other than the mechanosensitive ion channels. Not all capsaicin-sensitive neurons are mechanosensitive, and gadolinium has no effect on capsaicin-induced calcium transient in sensory neurons (Gschossmann et al., 2000). Depletion of group IV fibers by neonatal capsaicin treatment reduces the influence of EA on the pressor responses to mechanical stimulation of visceral organs (Tjen-A-Looi et al., 2005), suggesting an importance of capsaicin-sensitive neurons in the mechanisms of acupuncture. Nociceptive neurons are therefore a likely candidate for the residual sensory mechanism after gadolinium administration. The group IV C-fiber tactile afferents is known to be widely distributed in the skin of mammals (Wessberg et al., 2003). These fibers could be regarded as a cutaneous intrinsic visceral afferent nervous system (Silberstein, 2009). In addition, the present results do not rule out the possibility that direct depolarization of sensory axons or nerve terminals occurs during EA. Albeit this assumption, EA seemed to have received even greater influence from gadolinium than MA (Figs. 1 and 2). Because MA with needle movements can cause greater deformations in the adjacent extracellular milieu compared to EA, MA may have induced signal transductions other than mechanosensitive ion channels, such as integrin-linked signal transduction pathways (Aplin et al., 1998), resulting in the greater residual hemodynamic responses after gadolinium administration. Further studies are required in the future to solve this question.

4.2. Effects of gadolinium on the AP and HR responses to ADN stimulation

Gadolinium decreased baseline AP, suggesting actions other than the inhibition of mechanosensitive ion channels. For instance, gadolinium has been shown to block voltage-gated calcium, sodium and potassium channels (Adding et al., 2001). To exclude the possibility that gadolinium attenuates the reflex hemodynamic responses to MA and EA via nonspecific mechanisms such as the inhibition of central autonomic neurotransmission, we performed the ADN stimulation experiment. Gadolinium did not attenuate ΔAP and ΔHR induced by ADN stimulation (Fig. 3). It is unlikely, therefore, that gadolinium inhibits the central autonomic neurotransmission from afferent to efferent nerve activities or significantly blunted the AP and HR responses to changes in autonomic nerve activities.

4.3. Implication of MA and EA

Although the present results indicate that MA and EA may share a common sensory mechanism, EA may be more flexible than MA in terms of its application for biomedical engineering because the effects of EA can be controlled quantitatively by adjusting the stimulation current and stimulation frequency. As an example, a previous study from our laboratories has demonstrated that servo-controlled hind limb electrical stimulation can reduce AP at a prescribed target level in anesthetized cats (Kawada et al., 2009). EA can be applied continuously using a stimulating device without the attendance of an acupuncturist once the needle is properly positioned. Continuous electrical stimulation of auricular acupuncture points for 48 h/week has been shown to be more effective than auricular acupuncture without electrical stimulation for the treatment of chronic cervical pain in an outpatient population (Sator-Katzenschlager et al., 2003). Although further studies are required, EA delivered via a dedicated stimulating device may be an additional modality to the treatment of cardiovascular diseases.

4.4. Limitations

First, the present study was conducted under pentobarbital anesthesia. Because anesthesia affects the autonomic tone, AP and HR

Please cite this article as: Yamamoto, H., et al., Involvement of the mechanoreceptors in the sensory mechanisms of manual and electrical acupuncture, Auton. Neurosci. (2010), doi:10.1016/j.autneu.2010.11.004

responses may differ when different anesthetics are used or when the animals are in a conscious state. However, as we compared the effects of gadolinium on the reflex responses to MA and EA under the same anesthetic conditions, the interpretation of the sensory mechanisms for MA and EA should be valid. Second, we performed EA at frequencies of 10 or 20 Hz in order to obtain AP and HR responses comparable to those observed during MA under control conditions. Because the effects of EA may differ depending on the magnitude of stimulation including pulse duration, current and frequency (Uchida et al., 2008; Kawada et al., 2009), further studies are needed to examine whether the effects of gadolinium on EA-induced hemodynamic responses vary depending on the stimulation intensities.

4.5. Conclusion

Intravenous administration of gadolinium attenuated the AP and HR responses to both MA and EA, suggesting that the mechanosensitive ion channels are involved in the sensory mechanisms of both MA and EA. EA may cause electrical twitching of surrounding tissues and induce MA-like stimulation through mechanoreceptors.

Acknowledgments

This study was supported by Health and Labour Sciences Research Grants (H19-nano-Ippan-009, H20-katsudo-Shitei-007, and H21-nano-Ippan-005) from the Ministry of Health, Labour and Welfare of Japan; by a Grant-in-Aid for Scientific Research (No. 20390462) from the Ministry of Education, Culture, Sports, Science and Technology of Japan; and by the Industrial Technology Research Grant Program from the New Energy and Industrial Technology Development Organization (NEDO) of Japan.

Appendix A

In an attempt to demonstrate that gadolinium does not significantly affect the hemodynamic responses to direct nerve stimulation related to acupuncture at the hind limb, we performed an additional protocol of tibial nerve stimulation in 5 anesthetized rats. The right tibial nerve was exposed and placed on a pair of platinum electrodes, and was stimulated for 120 s (500 μs, 10 Hz, 2 or 5 mA). ΔAP was -10.5 ± 3.5 mm Hg under baseline conditions, which was attenuated to -8.2 ± 4.4 mm Hg after gadolinium administration ($74 \pm 15\%$ of the pre-gadolinium, $P<0.01$). Although the relative reduction seemed smaller than that observed in EA ($38 \pm 11\%$ of the pre-gadolinium, see main text), because the reduction of ΔAP could be partly attributable to the decreased baseline AP after gadolinium administration, we could not judge whether gadolinium had truly inhibited the hypotensive effect of tibial nerve stimulation. Unfortunately, the tibial nerve stimulation did not change HR significantly in our experimental conditions ($\Delta HR = -1.1 \pm 4.4$ bpm before gadolinium vs. $\Delta HR = -1.4 \pm 4.1$ bpm after gadolinium), as opposed to a previous study (Uchida et al., 2008). As a result, we could not judge the effect of gadolinium based on HR either. We think the ADN stimulation protocol in the main text would be a second best surrogate to indicate the inability of gadolinium to block hemodynamic responses induced by direct activation of the afferent nerve.

References

Adding, L.C., Bannenberg, G.L., Gustafsson, L.E., 2001. Basic experimental studies and clinical aspects of gadolinium salts and chelates. Cardiovasc. Drug Rev. 19, 41–56.
Aplin, A.E., Howe, A., Alahari, S.K., Juliano, R.L., 1998. Signal transduction and signal modulation by cell adhesion receptors: the role of integrins, cadherins, immunoglobulin-cell adhesion molecules, and selectins. Pharmacol. Rev. 50 (2), 197–263.
Burnstock, G., 2009. Acupuncture: a novel hypothesis for the involvement of purinergic signalling. Med. Hypotheses 73, 470–472.
Cho, H., Shin, J., Shin, C.Y., Lee, S., Oh, U., 2002. Mechanosensitive ion channels in cultured sensory neurons of neonatal rats. J. Neurosci. 22 (4), 1238–1247.
Glantz, S.A., 2002. Primer of Biostatistics, 5th ed. McGraw-Hill, New York.
Gschossmann, J.M., Chaban, V.V., McRoberts, J.A., Raybould, H.E., Young, S.H., Ennes, H.S., Lembo, T., Mayer, E.A., 2000. Mechanical action of dorsal root ganglion cells in vitro: comparison with capsaicin and modulation by kappa-opioids. Brain Res. 856 (1–2), 101–110.
Kawada, T., Shimizu, S., Yamamoto, T., Shishido, T., Kamiya, A., Miyamoto, T., Sunagawa, K., Sugimachi, M., 2009. Servo-controlled hind-limb electrical stimulation for short-term arterial pressure control. Circ. J. 73 (5), 851–859.
Kimura, A., Sato, A., 1997. Somatic regulation of autonomic functions in anesthetized animals—neural mechanisms of physical therapy including acupuncture. Jpn J. Vet. Res. 45 (3), 137–145.
Langevin, H.M., Churchill, D.L., Cipolla, M.J., 2001. Mechanical signaling through connective tissue: a mechanism for the therapeutic effect of acupuncture. FASEB J. 15, 2275–2285.
Lin, M.C., Nahin, R., Gershwin, M.E., Longhurst, J.C., Wu, K.K., 2001. State of complementary and alternative medicine in cardiovascular, lung, and blood research: executive summary of a workshop. Circulation 103 (16), 2038–2041.
Nakamoto, T., Matsukawa, K., 2007. Muscle mechanosensitive receptors close to the myotendinous junction of the Achilles tendon elicit a pressor reflex. J. Appl. Physiol. 102, 2112–2120.
Napadow, V., Makris, N., Liu, J., Kettner, N.W., Kenneth, K.K., Hui, K.K.S., 2005. Effects of electroacupuncture versus manual acupuncture on the human brain as measured by fMRI. Hum. Brain Mapp. 24, 193–205.
Sato, A., Sato, Y., Schmidt, R.F., 1981. Heart rate changes reflecting modifications of efferent cardiac sympathetic outflow by cutaneous and muscle afferent volleys. J. Auton. Nerv. Syst. 4 (3), 231–247.
Sato, A., Sato, Y., Suzuki, A., Uchida, S., 1994. Reflex modulation of gastric and vesical function by acupuncture-like stimulation in anesthetized rats. Biomed. Res. 15, 59–65.
Sato, A., Sato, Y., Uchida, S., 2002. Reflex modulation of visceral functions by acupuncture-like stimulation in anesthetized rats. Int. Congr. Ser. 1238, 111–123.
Sator-Katzenschlager, S.M., Szeles, J.C., Scharbert, G., Michalek-Sauberer, A., Kober, A., Heinze, G., Kozek-Langenecker, S.A., 2003. Electrical stimulation of auricular acupuncture points is more effective than conventional manual auricular acupuncture in chronic cervical pain: a pilot study. Anesth. Analg. 97, 1469–1473.
Silberstein, M., 2009. The cutaneous intrinsic visceral afferent nervous system: a new model for acupuncture analgesia. J. Theor. Biol. 261, 637–642.
Tjen-A-Looi, S.C., Fu, L.-W., Zhou, W., Syuu, Z., Longhurst, J.C., 2005. Role of unmyelinated fibers in electroacupuncture cardiovascular responses. Auton. Neurosci. 118, 43–50.
Uchida, S., Shimura, M., Ohsawa, H., Suzuki, A., 2007. Neural mechanism of bradycardic responses elicited by acupuncture-like stimulation to a hind limb in anesthetized rats. J. Physiol. Sci. 57 (6), 377–382.
Uchida, S., Kagitani, F., Hotta, H., 2008. Mechanism of the reflex inhibition of heart rate elicited by acupuncture-like stimulation in anesthetized rats. Auton. Neurosci. 143, 12–19.
Wessberg, J., Olausson, H., Fernstrom, W.F., Vallbo, B.A., 2003. Receptive field properties of unmyelinated tactile afferents in the human skin. J. Neurophysiol. 89, 1567–1575.
Yamamoto, H., Kawada, T., Kamiya, A., Kita, T., Sugimachi, M., 2008. Electroacupuncture changes the relationship between cardiac and renal sympathetic nerve activities in anesthetized cats. Auton. Neurosci. 144 (1–2), 43–49.

Please cite this article as: Yamamoto, H., et al., Involvement of the mechanoreceptors in the sensory mechanisms of manual and electrical acupuncture, Auton. Neurosci. (2010), doi:10.1016/j.autneu.2010.11.004

Am J Physiol Heart Circ Physiol 298: H1966–H1975, 2010.
First published March 26, 2010; doi:10.1152/ajpheart.00340.2009.

Parallel resetting of arterial baroreflex control of renal and cardiac sympathetic nerve activities during upright tilt in rabbits

Atsunori Kamiya, Toru Kawada, Masaki Mizuno, Shuji Shimizu, and Masaru Sugimachi
Department of Cardiovascular Dynamics, National Cardiovascular Centre Research Institute, Suita, Japan

Submitted 8 April 2009; accepted in final form 23 March 2010

Kamiya A, Kawada T, Mizuno M, Shimizu S, Sugimachi M. Parallel resetting of arterial baroreflex control of renal and cardiac sympathetic nerve activities during upright tilt in rabbits. *Am J Physiol Heart Circ Physiol* 298: H1966–H1975, 2010. First published March 26, 2010; doi:10.1152/ajpheart.00340.2009.—Since humans are under ceaseless orthostatic stress, the mechanisms to maintain arterial pressure (AP) against gravitational fluid shift are important. As one mechanism, it was reported that upright tilt reset baroreflex control of renal sympathetic nerve activity (SNA) to a higher SNA in anesthetized rabbits. In the present study, we tested the hypothesis that upright tilt causes a parallel resetting of baroreflex control of renal and cardiac SNAs in anesthetized rabbits. In anesthetized rabbits (n = 8, vagotomized and aortic denervated) with 0° supine and 60° upright tilt postures, renal and cardiac SNAs were simultaneously recorded while isolated intracarotid sinus pressure (CSP) was increased stepwise from 40 to 160 mmHg with increments of 20 mmHg. Upright tilt shifted the reverse-sigmoidal curve of the CSP-SNA relationship to higher SNA similarly in renal and cardiac SNAs. Although upright tilt increased the maximal gain, the response range and the minimum value of SNA, the curves were almost superimposable in these SNAs regardless of postures. Scatter plotting of cardiac SNA over renal SNA during the stepwise changes in CSP was close to the line of identity in 0° supine and 60° upright tilt postures. In addition, upright tilt also shifted the reverse-sigmoidal curve of the CSP-heart rate relationship to a higher heart rate, with increases in the maximal gain and the response range. In conclusion, upright posture caused a resetting of arterial baroreflex control of SNA similarly in renal and cardiac SNAs in anesthetized rabbits.

blood pressure; orthostasis; sympathetic nervous system

SINCE HUMANS ARE UNDER CEASELESS orthostatic stress, the mechanisms to maintain arterial pressure (AP) against gravitational fluid shift are greatly important. During standing, a gravitational fluid shift directed toward the lower part of the body (such as the abdominal vascular bed and lower limbs) will cause severe postural hypotension if not counteracted by compensatory mechanisms (15). Arterial baroreflexes have been considered to be the major compensatory mechanism (1, 13, 15), since denervation of baroreceptor afferents causes profound postural hypotension (16). In addition, we (8) recently reported that upright tilt resets baroreflex control of sympathetic nerve activity (SNA) to higher SNA. The resetting doubles SNA, compensates for the reduced pressor responses of cardiovascular organs to SNA during gravitational stress, and contributes to prevent postural hypotension. However, since the study recorded only renal SNA, it remains unknown whether upright tilt resets arterial baroreflex control of SNA innervating cardiovascular organs (i.e., the heart) other than the kidney. Since cardiac SNA has a critical role in circulation, baroreflex control of cardiac SNA during orthostatic stress is of importance.

Accordingly, in the present study, we tested the hypothesis that upright tilt causes a parallel resetting of arterial baroreflex control of renal and cardiac SNAs in anesthetized rabbits. Since total baroreflex is a closed-loop negative feedback system that senses baroreceptor pressure and controls AP, and since the baroreflex control of SNA (from baroreceptor pressure input to SNA) is a subsystem of the total baroreflex system, it is difficult to isolate the baroreflex control of SNA from the total system in the baroreflex closed-loop condition (16). Therefore, we opened the baroreflex feedback loop by vascularly isolating the carotid sinus region and loaded artificial stepwise intracarotid sinus pressure (CSP) in anesthetized rabbits. By recording renal and cardiac SNAs simultaneously, we investigated static characteristics of baroreflex control of these SNAs (CSP-SNA relationship) in 0° and 60° upright tilt postures.

METHODS

Animals, preparation, and measurements. Japanese White rabbits weighing 2.4–3.3 kg were used. Animals were cared for in strict accordance with the "Guiding Principles for the Care and Use of Animals in the Field of Physiological Science" approved by the Physiological Society of Japan.

Animals (n = 8) were initially anesthetized by intravenous injection (2 ml/kg) of a mixture of urethane (250 mg/ml) and α-chloralose (40 mg/ml). Anesthesia was maintained by continuously infusing the anesthetics at a rate of 0.33 $ml \cdot kg^{-1} \cdot h^{-1}$ using a syringe pump (CFV-3200; Nihon Kohden, Tokyo, Japan). The rabbits were mechanically ventilated with oxygen-enriched room air. Bilateral carotid sinuses were isolated vascularly from the systemic circulation by ligating the internal and external carotid arteries and other small branches originating from the carotid sinus regions. The isolated carotid sinuses were filled with warmed physiological saline, pre-equilibrated with atmospheric air, through catheters inserted via the common carotid arteries. The intracarotid sinus pressure (CSP) was controlled by a servo-controlled piston pump (model ET-126A; Labworks, Costa Mesa, CA). Bilateral vagal and aortic depressor nerves were sectioned in the middle of the neck region to eliminate reflexes from the cardiopulmonary region and the aortic arch. The systemic AP was measured using a high-fidelity pressure transducer (Millar Instruments, Houston, TX) inserted retrograde from the right common carotid artery below the isolated carotid sinus region. Heart rate (HR) was measured with a cardiotachometer (model N4778; San-ei, Tokyo, Japan).

Body temperature was maintained at around 38°C with a heating pad. The left renal sympathetic nerve was exposed retroperitoneally, and the left cardiac sympathetic nerve was exposed through a middle thoracotomy. A pair of stainless steel wire electrodes (Bioflex wire AS633; Cooner Wire) was hooked onto each of these nerves to record renal and cardiac SNAs. The nerve fibers peripheral to electrodes were ligated securely and crushed to eliminate afferent signals. The nerve

Address for reprint requests and other correspondence: A. Kamiya, Dept. of Cardiovascular Dynamics, National Cardiovascular Centre Research Institute, Suita 565-8565, Japan (e-mail: kamiya@ri.ncvc.go.jp).

and electrodes were covered with a mixture of silicone gel (silicon low viscosity, Kwik-Sil; World Precision Instruments, Sarasota, FL) to insulate and immobilize the electrodes. The preamplified SNA signals were band-pass filtered at 150–1,000 Hz. These nerve signals were full-wave rectified and low-pass filtered with a cutoff frequency of 30 Hz to quantify the nerve activity. After the experiment, an intravenous infusion of hexamethonium bromide (6 mg/kg) abolished the SNA signals, indicating that the signals recorded were postganglionic SNA.

Protocols. After the preparation, the animal was maintained in a 0° supine posture on a tilt bed. To stabilize the posture, the head was fixed full-frontal to the bed by strings, and the body and legs were rigged up in a clothes-like bag. Bilateral CSP was artificially controlled independently of systemic AP. First, actual operating pressure and SNAs under baroreflex closed-loop conditions in the 0° supine posture were obtained. The animal was kept in the 0° supine posture for 10 min while CSP was matched with systemic AP via the servo-controlled piston pump.

Second, the static characteristics of the sympathetic baroreflex system were estimated in the 0° position under baroreflex open-loop conditions. The animal was kept in the 0° supine posture while CSP was decreased to 40 mmHg and then increased stepwise from 40 to 160 mmHg in increments of 20 mmHg. Each CSP step was maintained for 60 s.

Third, actual operating pressure and SNAs under baroreflex closed-loop conditions in the 60° upright tilt position were obtained. The animal was kept supine for 10 min and then tilted upright to 60° within 10 s by inclining the tilt bed to 60° and dropping the lower regions of the rabbit with the fulcrum set at the level of the carotid sinus. The 60° upright posture was maintained for 10 min. CSP was matched with systemic AP via the servo-controlled piston pump. Since the clothes-like bag stabilized the posture of the animals, there was no additional mechanical movement that reduced the quality of measurements. The position of the head remained almost fixed during the tilt to minimize vestibular stimulation. Last, the static characteristics of the sympathetic baroreflex system were estimated during the 60° upright tilt posture. CSP was increased stepwise from 40 to 160 mmHg similarly to the experiment in the 0° position. These SNAs and AP were recorded at a 200-Hz sampling rate using a 12-bit analog-to-digital converter and stored on the hard disk of a dedicated laboratory computer system for later analysis.

Data analysis. The SNA signals were normalized by the following steps. First, for each type of SNA, 0 arbitrary unit (a.u.) was assigned to the postmortem noise level. Second, 100 a.u. were assigned to the average of actual operating SNA values during baseline period in 0° positions. Last, the other SNA signals were then normalized to these values in each experiment.

These SNA and HR values were averaged for the last 10 s of each CSP level. The static relationships between CSP and SNA and between CSP and HR were parameterized by two widely used traditional models (nonlinear reverse-sigmoidal curve, linear regression line), although both models have limited abilities to reproduce the actual data. In the former case, the data were parameterized by a four-parameter logistic equation model as follows:

$$Y = P_4 + \frac{P_1}{1 + \exp[P_2(CSP - P_3)]} \quad (1)$$

where Y is SNA or HR, P_1 is the response range of Y (i.e., the difference between the maximum and minimum values of Y), P_2 is the coefficient of gain, P_3 is the midpoint CSP of the logistic function, and P_4 is the minimum value of Y. We calculated the instantaneous gain

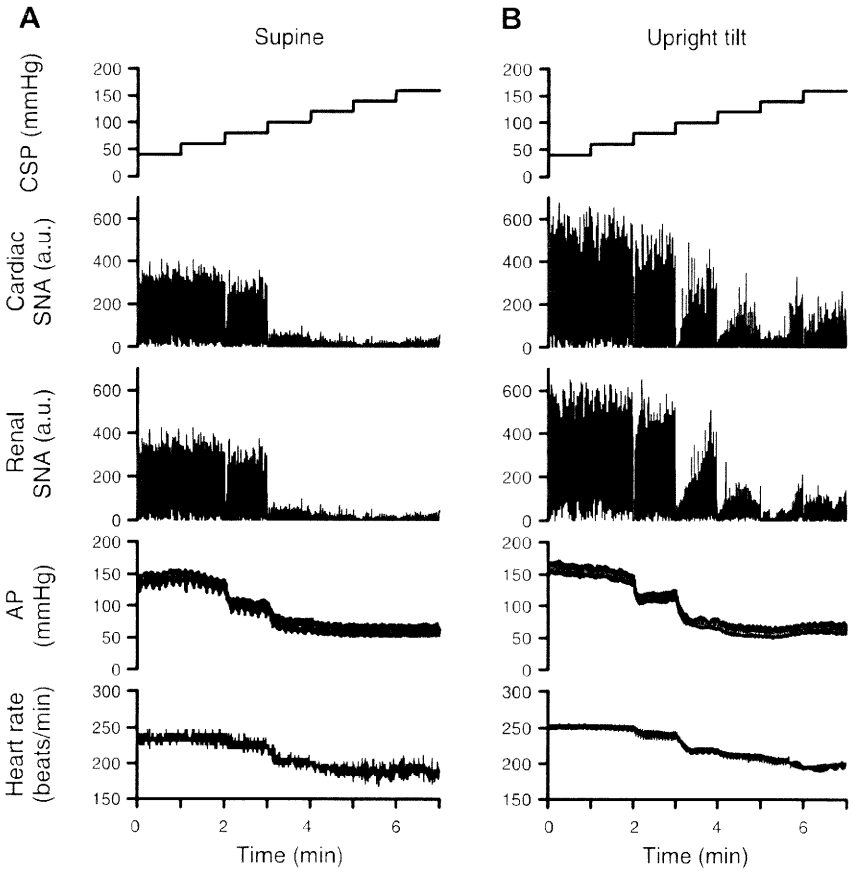

Fig. 1. Representative time series of renal and cardiac sympathetic nerve activities (SNAs) and arterial pressure (AP) in response to a stepwise increase in intracarotid sinus pressure (CSP) in 0° supine (*A*) and 60° upright tilt postures (*B*) obtained from 1 animal. Each CSP step was maintained for 1 min. All data were sampled at 10 Hz. In both SNAs, increasing CSP decreased SNAs in both postures, but upright tilt increased SNAs at all CSP levels. a.u., Arbitrary unit.

from the first derivative of the logistic function and the maximum gain (G_{max}) from $-P_1P_2/4$ at CSP = P_3.

Statistic analysis. All data are means ± SD. Effects of the upright tilt on baroreflex parameters were evaluated by repeated-measures analysis of variance. When the main effect was found to be significant, post hoc multiple comparisons were made using Scheffé's *F*-test to compare baroreflex controls between renal and cardiac SNAs (3). Differences were considered significant when $P < 0.05$.

RESULTS

Baroreflex control of renal and cardiac SNAs. Figure 1 shows the representative time series data obtained from one subject. The renal and cardiac SNAs similarly decreased in response to stepwise increase in CSP in the 0° supine posture (Fig. 1*A*). The 60° upright tilt increased these SNAs at each CSP level (Fig. 1*B*) compared with the supine posture.

Figure 2 shows the relationship between CSP and SNA in the same data as in Fig. 1*A*. In Fig. 2, these SNAs were averaged for the last 10 s of each CSP level to investigate the steady-state, not transient, response to a stepwise change in CSP. The 60° upright tilt increased renal (Fig. 2*A*) and cardiac SNAs (Fig. 2*C*) at all CSP levels compared with the supine posture. The renal SNA approximately matched the cardiac SNA at all CSP levels in the supine posture (Fig. 2*B*) and also in the upright tilt posture (Fig. 2*D*).

When the static relationship between CSP and each SNA was fitted to a nonlinear reverse-sigmoidal curve (Fig. 3), the r^2 value was ~0.95. The 60° upright tilt shifted the CSP-renal SNA curve upward to a higher SNA (Fig. 3*A*). Similarly, the upright tilt shifted the CSP-cardiac SNA curve (Fig. 3*C*) in the same manner as renal SNA. The CSP-renal SNA curve was almost superimposed on the CSP-cardiac SNA curve in the 0° supine (Fig. 3*B*) and upright tilt postures (Fig. 3*D*). However, the model was limited in reproducing the data, since the measured SNAs did not saturate at the CSP levels of 40–60 mmHg.

When the static relationship between CSP and each SNA was fitted to a linear regression line (Fig. 4), the r^2 value was 0.82–88, lower than when the nonlinear reverse-sigmoidal curve was used. The 60° upright tilt shifted the CSP-renal SNA (Fig. 4*A*) and the CSP-cardiac SNA lines (Fig. 4*C*) upward to the higher SNA levels. The CSP-renal SNA line was almost superimposed on the CSP-cardiac SNA line in the 0° supine (Fig. 4*B*) and upright tilt postures (Fig. 4*D*).

Averaged data from all animals showed that the 60° upright tilt increased renal (Fig. 5*A*) and cardiac SNAs (Fig. 5*B*) at all CSP levels compared with the 0° supine posture. The renal SNA almost matched the cardiac SNA at all CSP levels in the supine (Fig. 5*D*) and also in the upright tilt posture (Fig. 5*E*),

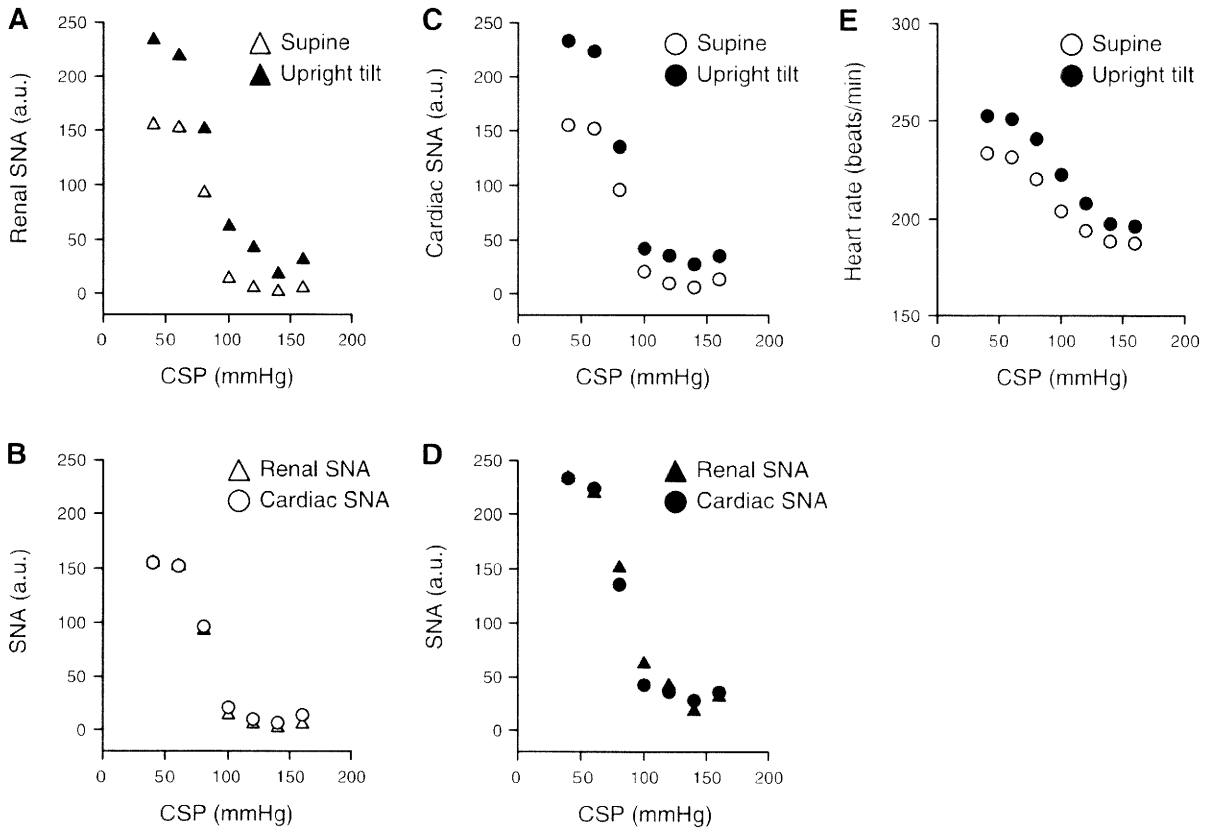

Fig. 2. Example of arterial baroreflex control of renal (*A*) and cardiac SNAs (*C*) and heart rate (HR; *E*). Data were obtained from the same animal studied in Fig. 1 and averaged for the last 10 s of each CSP level. Open and filled symbols show the data in the supine and 60° upright tilt postures, respectively. The upright tilt shifted the baroreflex control of SNA to a higher SNA similarly in the CSP-renal SNA (*A*) and CSP-cardiac SNA relationships (*C*). Data in *B* and *D* represent the superimposing of baroreflex control of SNA between renal and cardiac SNAs in both the supine and upright tilt postures, respectively. The upright tilt also shifted the baroreflex control of HR upward (*E*).

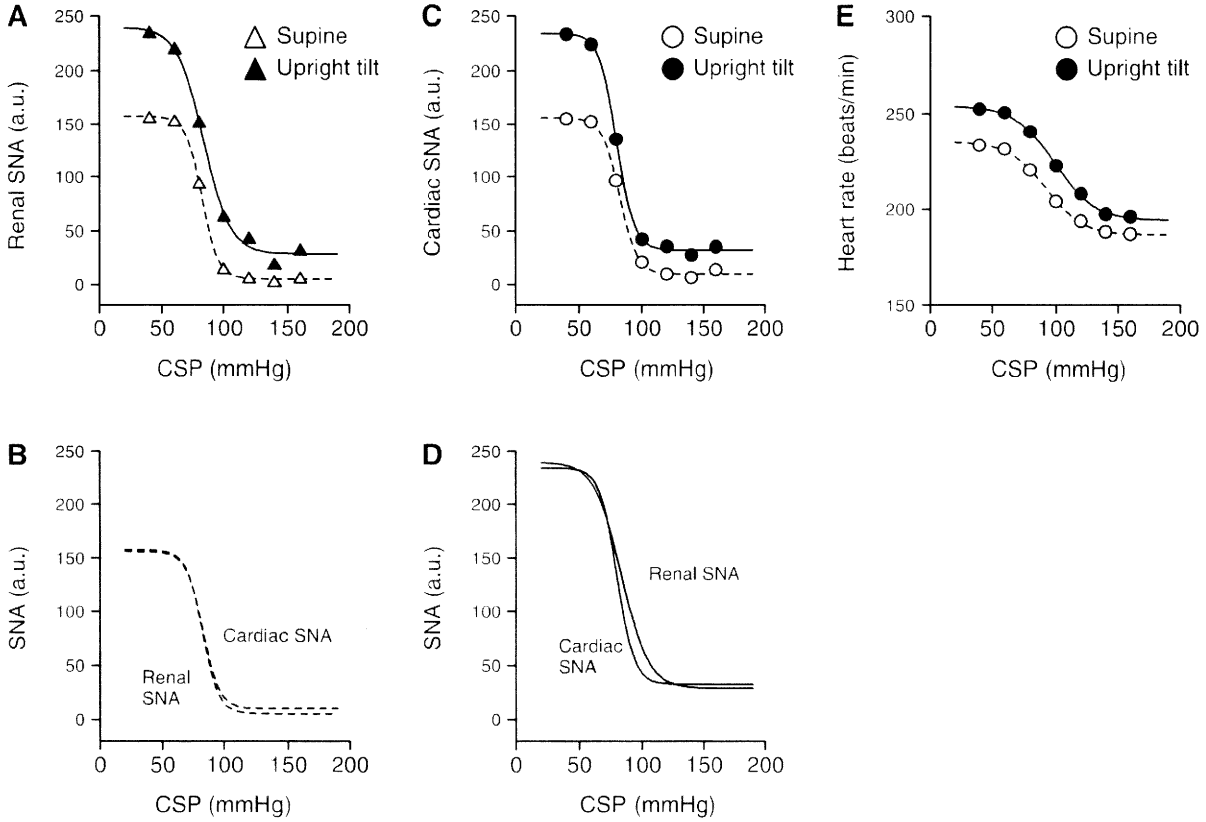

Fig. 3. Example of a model of the data shown in Fig. 2 using reverse-sigmoid 4-parameter logistic functions. Dotted and solid curves show the data in the supine and 60° upright tilt postures, respectively. The upright tilt shifted the baroreflex curves to a higher SNA similarly in renal (*A*) and cardiac SNAs (*C*). The curves were superimposed between these SNAs in the supine (*B*) and upright tilt postures (*D*). The upright tilt also shifted the baroreflex curve of HR upward (*E*).

indicating that 60° upright tilt shifted the CSP-SNA relationship upward by similar magnitudes in renal and cardiac SNAs.

When the static relationship between CSP and each SNA was fitted to a nonlinear reverse-sigmoidal curve (Fig. 6), the upright tilt shifted the CSP-SNA curve to higher SNA similarly in renal (Fig. 6*A*) and cardiac SNAs (Fig. 6*C*). The CSP-SNA relationship was almost superimposed between these SNAs in both the supine (Fig. 6*B*) and upright tilt postures (Fig. 4*D*). In both renal and cardiac SNAs, P_1 (the range of SNA response to CSP), P_4 (the minimum value of SNA), and the maximal gain (at the midpoint of the logistic function) were larger at upright tilt than supine posture (Table 1), whereas P_2 (the coefficient of gain) and P_3 (the midpoint CSP of the logistic function) were not different between postures (Table 1). In both postures, these parameters of P_{1-4} and maximal gain were similar in renal and cardiac SNAs (Table 1).

When the static relationship between CSP and each SNA was fitted to a linear regression line (Fig. 7), the upright tilt shifted the CSP-SNA line to higher SNA similarly in renal (Fig. 7*A*) and cardiac SNAs (Fig. 7*C*). It increased the slope of regression from -1.4 ± 0.3 to -1.8 ± 0.3 a.u./mmHg in renal SNA and from -1.4 ± 0.3 to -1.8 ± 0.4 a.u./mmHg in cardiac SNA. The CSP-SNA lines were almost superimposed on their SNAs in the 0° supine (Fig. 7*B*) and also the upright tilt posture (Fig. 7*D*). In both SNAs of all animals, the r^2 value was always lower (0.80–0.89) than when a nonlinear reverse-sigmoidal curve was used (0.92–0.97).

In addition, in both 0° supine and 60° upright tilt postures, scatter plotting of cardiac SNA over renal SNA was approximately close to the line of identity for each subject (Fig. 8A) and the pooled data from all subjects (Fig. 8*B*), indicating that these SNAs changed in parallel in response to stepwise increase in CSP regardless of posture. The upright tilt did not change operating AP (steady-state AP: 102 ± 4 mmHg in supine posture, 102 ± 5 mmHg in upright tilt posture). The upright tilt increased operating renal (100 a.u in supine posture, 148 ± 19 a.u. in upright posture) and cardiac SNAs (100 a.u in supine posture, 155 ± 21 a.u. in upright posture) by similar magnitudes.

Figure 9 showed the discharge characteristics of the renal and cardiac SNAs obtained from the same animal studied in Fig. 1. These SNAs were similar to some extent regardless of baroreflex condition and posture. In the supine posture (Fig. 9*A*), first, these SNAs were weakly pulse synchronous and had slower fluctuations with a time cycle of ~1.7 s in the baroreflex closed-loop condition, where CSP was artificially matched with systemic AP. The CSP and AP also had fluctuations with the same time cycle. Second, in the baroreflex open-loop condition, where CSP was fixed at 40 mmHg (the CSP level was chosen because it maximized these SNAs) without pulse, these SNAs had neither a pulse rhythmicity nor the slower fluctuation observed in the closed-loop condition. These discharge characteristics of SNAs were also observed in the 60° upright posture (Fig. 9*B*), although the amplitude of SNAs were larger at upright tilt than supine posture.

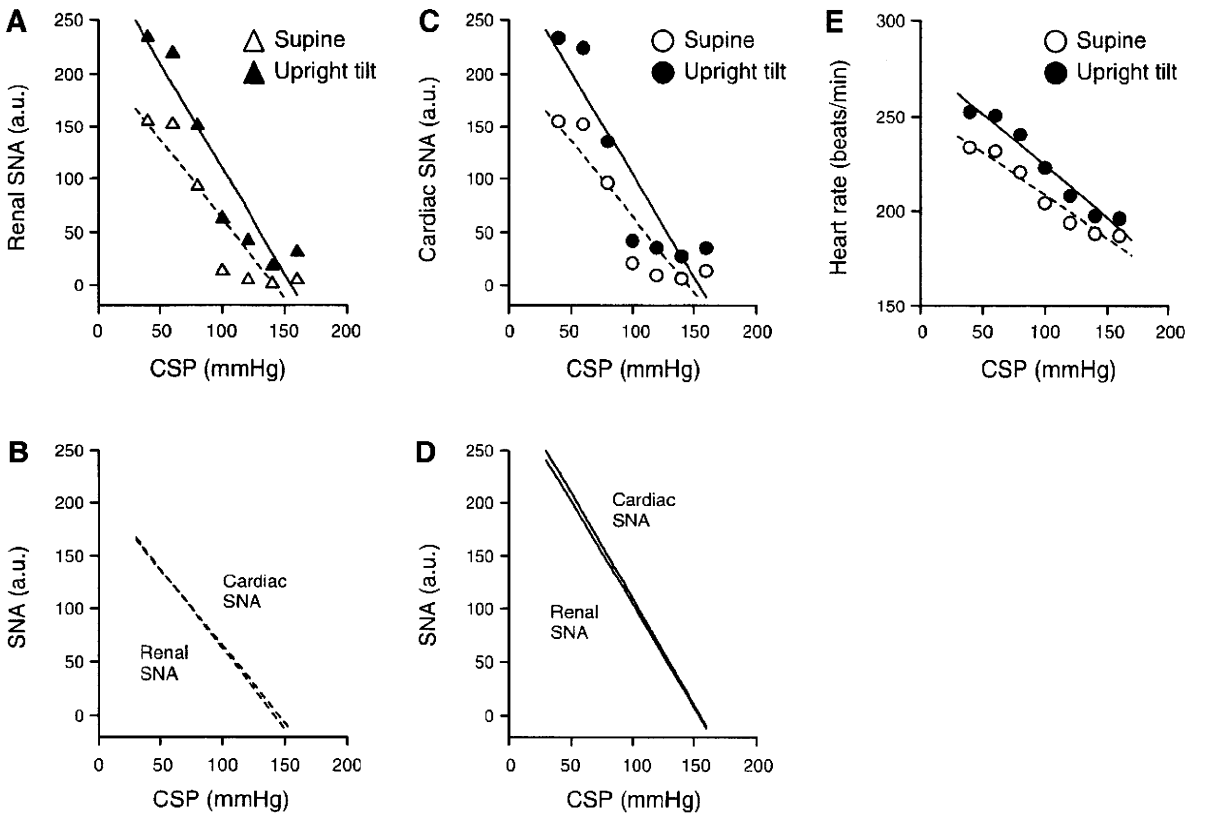

Fig. 4. Example of a model of the data shown in Fig. 2 using a simple regression line. Dotted and solid lines show the data in the supine and 60° upright tilt postures, respectively. The upright tilt shifted the baroreflex lines to a higher SNA similarly in renal (*A*) and cardiac SNAs (*C*). The lines were superimposed between these SNAs in the supine (*B*) and upright tilt postures (*D*). The upright tilt also shifted the baroreflex line of HR upward (*E*).

Baroreflex control of HR. In the representative time-series data, HR decreased in response to a stepwise increase in CSP in the 0° supine posture (Fig. 1*A*) and during 60° upright tilt (Fig. 1*B*). The upright tilt shifted the CSP-HR relationship upward to a higher HR (Fig. 2*E*), although HR was averaged for the last 10 s of each CSP level to investigate the steady-state, not transient, response to stepwise change in CSP.

Averaged data from all animals showed that the upright tilt shifted the CSP-HR relationship upward to a higher HR (Fig. 5*E*). When the static relationship between CSP and HR was fitted to a nonlinear reverse-sigmoidal curve (Fig. 6*E*), the P_1 (the range of HR response to CSP) and the maximal gain (at the midpoint of the logistic function) were larger at upright tilt than in the supine posture (Table 2), whereas P_2 (the coefficient of gain), P_3 (the midpoint CSP of the logistic function), and P_4 (the minimum value of HR) were not different between postures (Table 2). When the static relationship between CSP and HR was fitted to a linear regression line (Fig. 8*E*), the upright tilt increased the slope of regression from 0.46 ± 0.3 to 0.60 ± 0.3 beats·min^{-1}·mmHg^{-1}. The upright tilt increased operating HR (steady-state HR; 204 ± 11 beats/min in supine posture, 220 ± 12 beats/min in upright tilt posture).

DISCUSSION

Arterial baroreflex control of SNA is considered to have an important role to maintain AP under orthostatic stress against gravitational fluid shift directed toward the lower part of the body (15). In addition, we (8) recently reported that upright tilt resets arterial baroreflex control of renal SNA to increase orthostatic sympathetic activation. However, it remains unknown whether upright tilt resets arterial baroreflex control of SNA innervating to cardiovascular organs (i.e., the heart) other than the kidney. One major new finding in this study is that 60° upright tilt resets arterial baroreflex control of SNA to higher SNA similarly in renal and cardiac SNAs. This supports our hypothesis that upright tilt causes a parallel resetting of arterial baroreflex control of renal and cardiac SNAs in anesthetized rabbits.

Some regional differences between renal and cardiac SNAs certainly have been reported under some physiological conditions. First, for example, the dynamic high-pass characteristics in baroreflex control of SNA were greater in cardiac SNA than renal SNA (6, 10). Second, activating left atrial receptors increased cardiac SNA but decreased renal SNA (9). Last, hypoxia reset the AP-SNA relationship to higher AP and SNA in renal SNA but to lower AP and SNA in cardiac SNA (4). These lines of evidence indicate that renal and cardiac SNAs respond differently to specific physiological stimulation and stress (14).

However, our results indicate that upright posture induces a parallel resetting in arterial baroreflex control of renal and cardiac SNAs in the static characteristics. In agreement with previous studies (6, 7), the CSP-renal SNA reverse-sigmoidal curve was superimposable to the CSP-cardiac SNA curve in

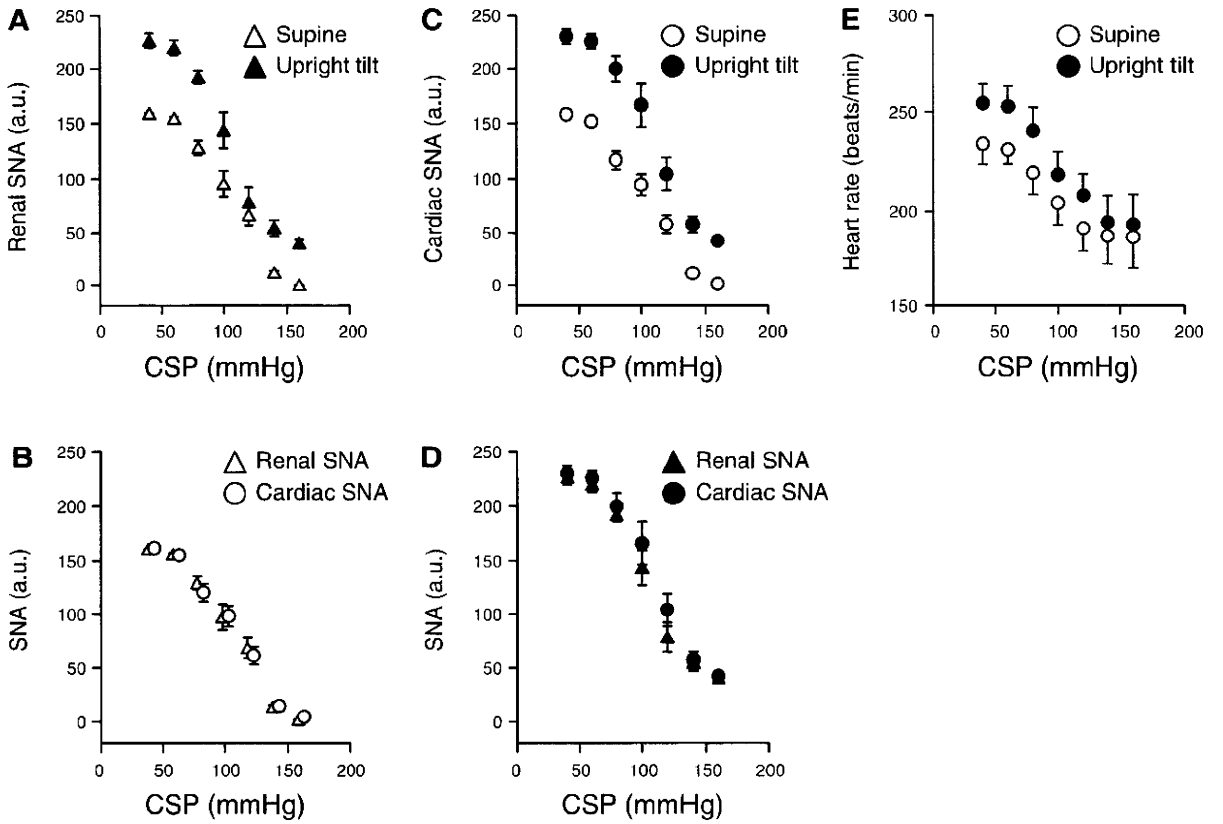

Fig. 5. Averaged data of arterial baroreflex control of renal (*A*) and cardiac SNAs (*C*) and HR (*E*) from all animals (n = 8). Open and filled symbols show the data in the supine and 60° upright tilt postures, respectively. The upright tilt shifted the baroreflex control of SNA to a higher SNA similarly in the CSP-renal SNA (*A*) and CSP-cardiac SNA relationships (*C*). *B* and *D* represent the superimposing of baroreflex control of SNA between renal and cardiac SNAs in both the supine and upright tilt postures, respectively. The upright tilt also shifted the baroreflex control of HR upward (*E*). Data are means ± SD.

the supine posture. This indicates that static nonlinear characteristics in arterial baroreflex control of renal SNA matched those of cardiac SNA in the posture. In addition, since upright tilt posture shifted the CSP-SNA curves upward similarly in renal and cardiac SNAs, the static nonlinear characteristics in arterial baroreflex control of renal SNA also matched those of cardiac SNA in upright tilt posture. These results were consistent with the close correlation between renal and cardiac SNAs during forced CSP changes with supine and upright tilt postures. They might also be consistent with a numerical simulation study indicating parallel responses of renal and cardiac SNAs to physiological pressure perturbations (AP change) (6).

Our results indicate that upright posture resets arterial baroreflex control of HR to a higher HR. This is consistent with the results of baroreflex resetting for cardiac SNA under upright tilt, because the P_1 (the response range) and the maximal gain (at the midpoint of the logistic function) were larger in both CSP-HR and CSP-cardiac SNA relationships. The parallelism suggests that cardiac sympathetic efferent was a dominant determinant for HR in the present experimental condition with cutting of vagal nerves. Our results could be consistent with the increase in the baroreflex gain for HR assessed by a neck pressure/suction device in humans (11).

Limitations. The present study has several limitations. First, we excluded the efferent effect of vagally mediated arterial baroreflex and an anesthetic agent that could affect baroreflex control of SNA. Second, the vascular isolation of carotid sinus might decrease brain blood flow under, in particular, upright tilt position. Third, we eliminated cardiopulmonary baroreflex by cutting bilateral vagal nerves. Earlier human studies have indicated that nonhypotensive hypovolemic perturbations do not change AP but reduce central venous, right heart, and pulmonary pressures and cause vasoconstriction. These observations have been interpreted as reflexes triggered by cardiopulmonary baroreceptors (5, 12). However, Taylor et al. (17) showed that small reductions of effective blood volume reduce aortic baroreceptive areas and trigger hemodynamic adjustments that are so efficient that alterations in AP escape detection by conventional means. In addition, Fu et al. (2) reported that arterial baroreceptors are consistently unloaded during low levels (i.e., −10 and −15 mmHg) of lower body negative pressure in humans. Accordingly, further studies are needed to understand the relative importance and mutual cooperation of arterial and cardiopulmonary baroreflexes in AP control during orthostatic stress. Fourth, we investigated arterial baroreflex during upright posture in rabbits, which are quadripeds. However, denervation of both carotid and aortic arterial baroreflexes caused postural hypotension of ~50 mmHg during 60° upright tilt in quadripeds [rabbits and rats (16)]. This suggests that even in quadripeds, arterial baroreflex has a very important role in maintenance of AP under orthostatic stress.

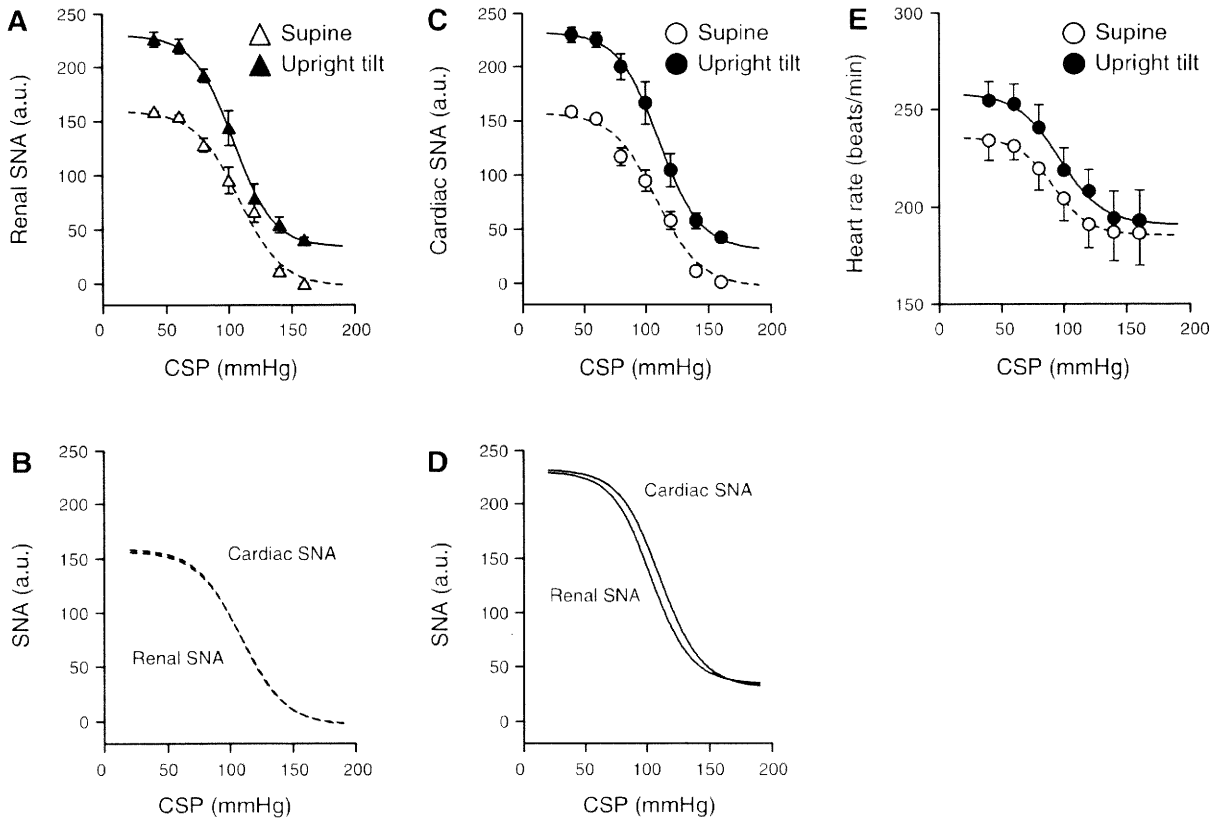

Fig. 6. A model of the averaged data shown in Fig. 5 using reverse-sigmoid 4-parameter logistic functions. Dotted and solid curves show the data in the supine and 60° upright tilt postures, respectively. The upright tilt shifted the baroreflex curves to a higher SNA similarly in renal (*A*) and cardiac SNAs (*C*). The curves were superimposed between these SNAs in the supine (*B*) and upright tilt postures (*D*). The upright tilt also shifted the baroreflex curve of HR upward (*E*).

Last, although we used two widely used traditional models to analyze the relationship between CSP and SNA, both have limited abilities to reproduce actual data. The nonlinear reverse-sigmoidal curve parameterized by a four-parameter logistic equation model provided high r^2 values (0.92–0.97) regardless of SNA type and posture. However, we failed to observe a saturation of SNA at the lowest CSP level in some cases (40 mmHg; Fig. 3, *A* and *B*, in upright tilt position). Lots of earlier studies have applied the model to AP and SNA (or HR) data under pharmacological perturbation (i.e., nitroprusside, phenylephrine) (1, 14), although it is difficult to observe clear saturation and/or threshold in the data. In contrary, the simple linear regression line model provided lower r^2 values (0.80–0.89). The plotted data did not appear to lie on a simple line in individuals (Fig. 4). Accordingly, we cannot conclude whether the relation between CSP and SNA is sigmoid or not. This problem is not the purpose of this study. Importantly, without modeling, our data (Fig. 2 and 5) indicate the parallel resetting of arterial baroreflex control of renal and cardiac SNAs.

Table 1. *Effect of upright tilt on parameters of baroreflex control of renal and cardiac SNAs*

	Supine	Upright tilt
Renal SNA		
P_1, a.u.	161 ± 2	196 ± 5*
P_2, a.u./mmHg	0.08 ± 0.01	0.08 ± 0.02
P_3, mmHg	105 ± 6	104 ± 6
P_4, a.u.	2 ± 1	34 ± 6*
G_{max}, a.u./mmHg	−1.5 ± 0.4	−1.9 ± 0.4*
Cardiac SNA		
P_1, a.u.	160 ± 2	201 ± 5*
P_2, a.u./mmHg	0.08 ± 0.01	0.08 ± 0.02
P_3, mmHg	109 ± 6	111 ± 6
P_4, a.u.	2 ± 1	31 ± 6*
G_{max}, a.u./mmHg	−1.4 ± 0.4	−1.9 ± 0.4*

Values are means ± SD (n = 8) for the parameters of baroreflex control of renal and cardiac sympathetic nerve activities (SNAs). See *Eq. 1* in METHODS for definitions of the 4 parameters of the logistic function. *$P < 0.05$, supine vs. upright tilt.

In conclusion, upright posture causes a resetting in arterial baroreflex control of SNA in parallel in renal and cardiac SNAs in anesthetized rabbits.

GRANTS

This study was supported by a research project promoted by the Ministry of Health, Labour and Welfare in Japan (no. H18-nano-ippan-003, H21-nano-ippan-005), a Grant-in-Aid for Scientific Research promoted by the Ministry of Education, Culture, Sports, Science and Technology in Japan (no. 20390462), and the Industrial Technology Research Grant Program from the New Energy and Industrial Technology Development Organization (NEDO) of Japan.

DISCLOSURES

No conflicts of interest, financial or otherwise, are declared by the author(s).

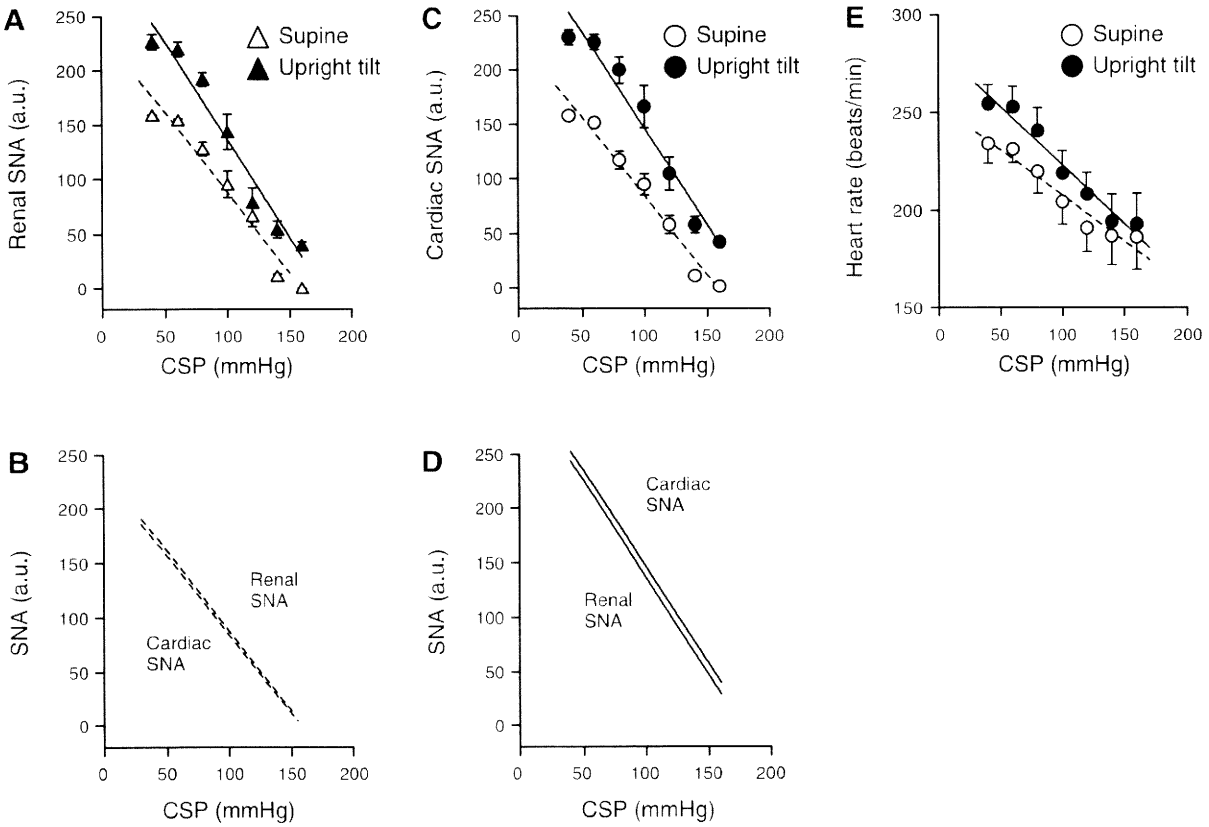

Fig. 7. A model of the averaged data shown in Fig. 5 using a simple regression line. Dotted and solid lines show the data in the supine and 60° upright tilt postures, respectively. The upright tilt shifted the baroreflex lines to a higher SNA similarly in renal (*A*) and cardiac SNAs (*C*). The lines were superimposed between these SNAs in the supine (*B*) and upright tilt postures (*D*). The upright tilt also shifted the baroreflex line of HR upward (*E*).

REFERENCES

1. **Eckberg DL, Sleight P.** *Human Baroreflexes in Health and Disease*. New York: Oxford Univ. Press, 1992, p. 3–299.
2. **Fu Q, Shibata S, Hastings JL, Prasad A, Palmer MD, Levine BD.** Evidence for unloading arterial baroreceptors during low levels of lower body negative pressure in humans. *Am J Physiol Heart Circ Physiol* 296: H480–H488, 2009.
3. **Glantz SA.** *Primer of Biostatistics* (4th ed.). New York: McGraw-Hill, 1997.
4. **Iriki M, Dorward P, Korner PI.** Baroreflex "resetting" by arterial hypoxia in the renal and cardiac sympathetic nerves of the rabbit. *Pflügers Arch* 370: 1–7, 1977.
5. **Johnson JM, Rowell LB, Niederberger M, Eisman MM.** Human splanchnic and forearm vasoconstrictor responses to reductions of right atrial and aortic pressures. *Circ Res* 34: 515–524, 1974.
6. **Kamiya A, Kawada T, Yamamoto K, Michikami D, Ariumi H, Miyamoto T, Shimizu S, Uemura K, Aiba T, Sunagawa K, Sugimachi M.** Dynamic and static baroreflex control of muscle sympathetic nerve activity (SNA) parallels that of renal and cardiac SNA during physiological change in pressure. *Am J Physiol Heart Circ Physiol* 289: H2641–H2648, 2005.
7. **Kamiya A, Kawada T, Yamamoto K, Michikami D, Ariumi H, Miyamoto T, Uemura K, Sugimachi M, Sunagawa K.** Muscle sympathetic nerve activity averaged over 1 min parallels renal and cardiac sympathetic nerve activity in response to a forced baroreceptor pressure change. *Circulation* 112: 384–386, 2005.
8. **Kamiya A, Kawada T, Yamamoto K, Michikami D, Ariumi H, Uemura K, Zheng C, Shimizu S, Aiba T, Miyamoto T, Sugimachi M, Sunagawa K.** Resetting of the arterial baroreflex increases orthostatic sympathetic activation and prevents postural hypotension in rabbits. *J Physiol* 566: 237–246, 2005.
9. **Karim F, Kidd C, Malpus CM, Penna PE.** The effects of stimulation of the left atrial receptors on sympathetic efferent nerve activity. *J Physiol* 227: 243–260, 1972.
10. **Kawada T, Shishido T, Inagaki M, Tatewaki T, Zheng C, Yanagiya Y, Sugimachi M, Sunagawa K.** Differential dynamic baroreflex regulation of cardiac and renal sympathetic nerve activities. *Am J Physiol Heart Circ Physiol* 280: H1581–H1590, 2001.
11. **Ogoh S, Yoshiga CC, Secher NH, Raven PB.** Carotid-cardiac baroreflex function does not influence blood pressure regulation during head-up tilt in humans. *J Physiol Sci* 56: 227–233, 2006.
12. **Pawelczyk JA, Raven PB.** Reductions in central venous pressure improve carotid baroreflex responses in conscious men. *Am J Physiol Heart Circ Physiol* 257: H1389–H1395, 1989.
13. **Persson P, Kirchheim H.** *Baroreceptor Reflexes: Integrative Functions and Clinical Aspects*. Berlin: Springer, 1991.
14. **Ramchandra R, Hood SG, Denton DA, Woods RL, McKinley MJ, McAllen RM, May CN.** Basis for the preferential activation of cardiac sympathetic nerve activity in heart failure. *Proc Natl Acad Sci USA* 106: 924–928, 2009.
15. **Rowell LB.** *Human Cardiovascular Control*. New York: Oxford Univ. Press, 1993, p. 3–254.
16. **Sato T, Kawada T, Sugimachi M, Sunagawa K.** Bionic technology revitalizes native baroreflex function in rats with baroreflex failure. *Circulation* 106: 730–734, 2002.
17. **Taylor JA, Halliwill JR, Brown TE, Hayano J, Eckberg DL.** "Non-hypotensive" hypovolaemia reduces ascending aortic dimensions in humans. *J Physiol* 483: 289–298, 1995.

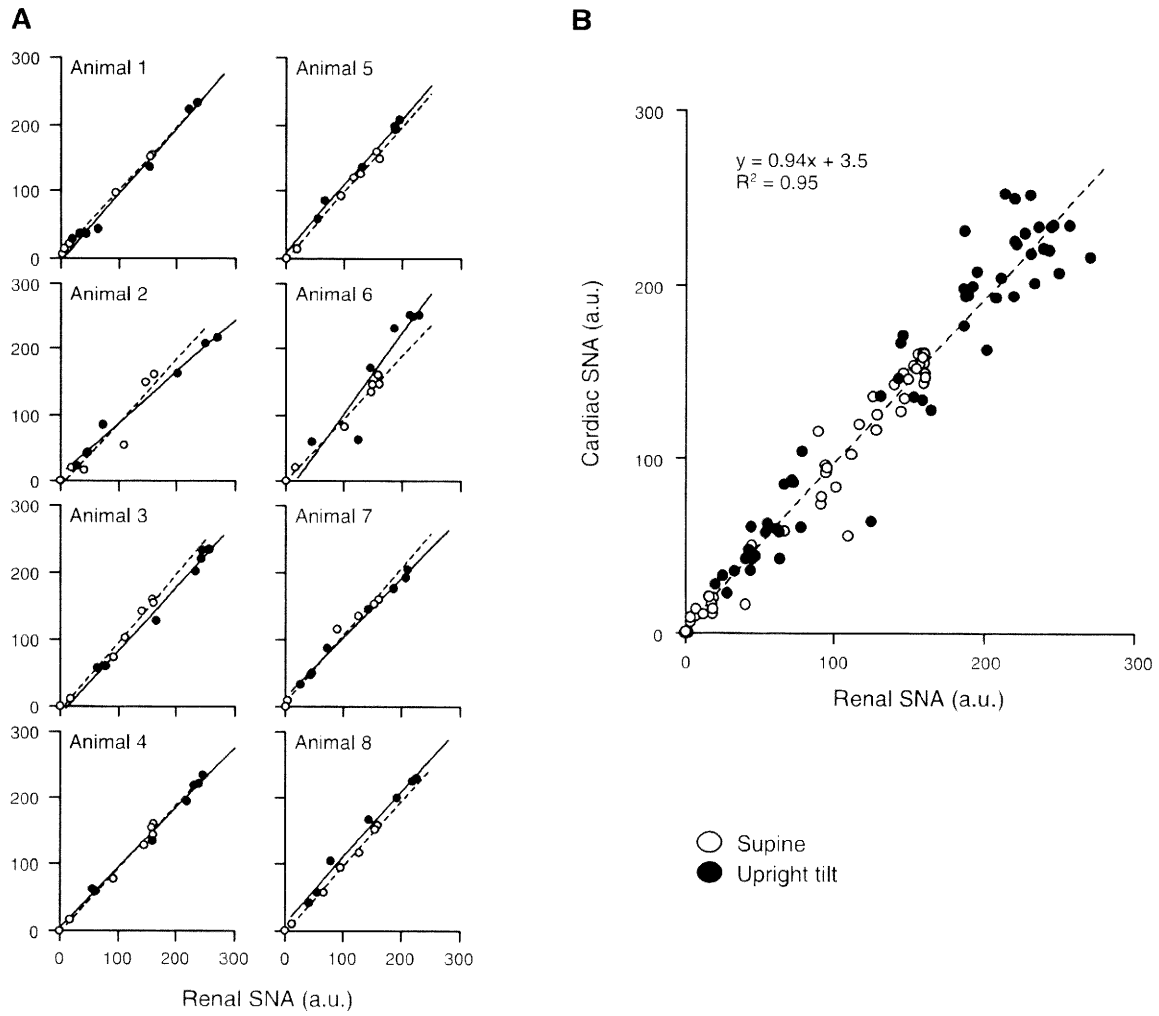

Fig. 8. Scatter plots and regression lines drawn between renal and cardiac SNAs in supine (dotted lines) and upright tilt postures (solid lines) during stepwise changes in CSP for each subject (*A*) and the pooled data from all 8 subjects (*B*).

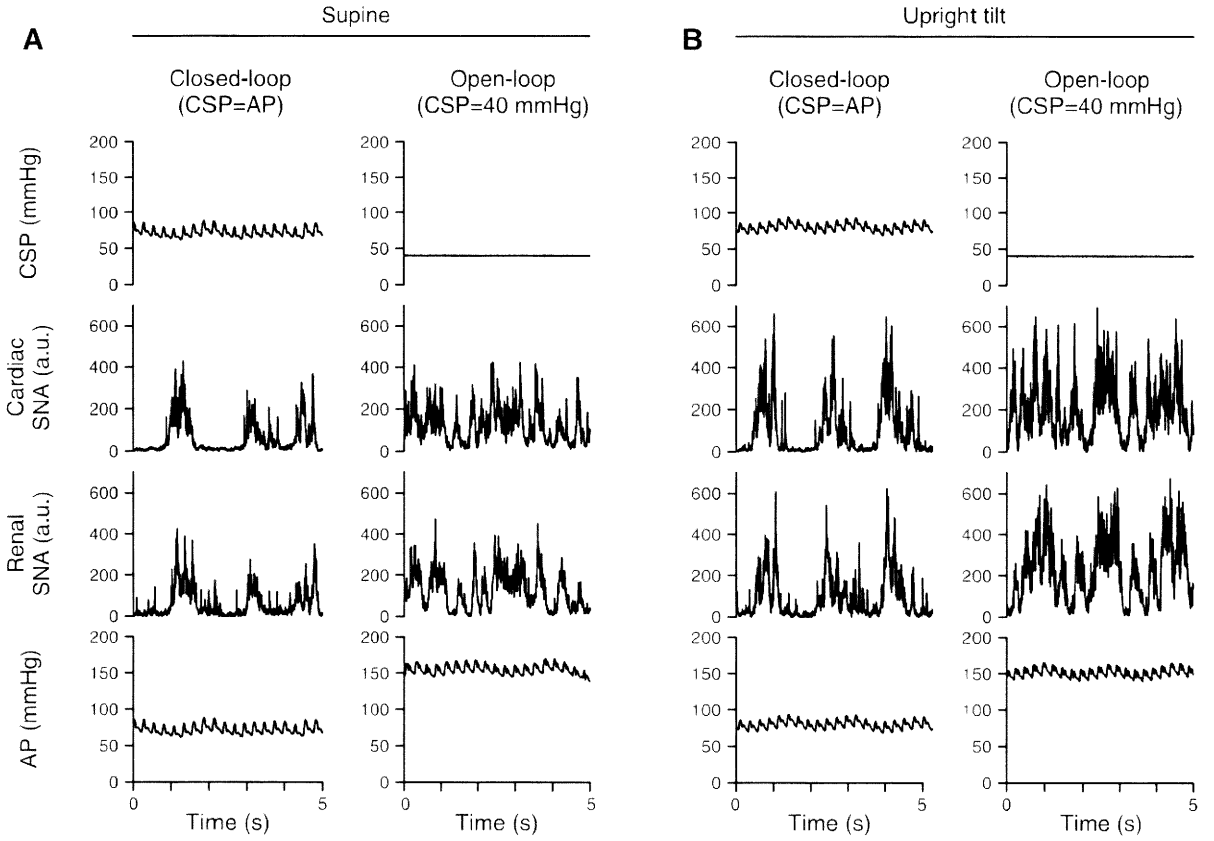

Fig. 9. Discharge characteristics of the renal and cardiac SNAs in supine (*A*) and 60° upright tilt postures (*B*) under the baroreflex closed-loop condition, where CSP was artificially matched with systemic AP, and under the open-loop condition, where CSP was fixed at 40 mmHg. Variables were resampled at 200 Hz. Data were obtained from the same animal studied in Fig. 1.

Table 2. *Effect of upright tilt on parameters of baroreflex control of HR*

	Supine	Upright tilt
P_1, beats/min	53 ± 11	67 ± 11*
P_2, beats·min^{-1}·mmHg^{-1}	0.07 ± 0.03	0.07 ± 0.03
P_3, mmHg	93 ± 8	97 ± 12
P_4, beats/min	184 ± 17	191 ± 18
G_{max}, beats·min^{-1}·mmHg^{-1}	−0.9 ± 0.2	−1.2 ± 0.4*

Values are means ± SD (n = 8) for the parameters of baroreflex control of heart rate (HR). *$P < 0.05$, supine vs. upright tilt.

J Physiol Sci (2010) 60:283–298
DOI 10.1007/s12576-010-0096-9

ORIGINAL PAPER

Open-loop dynamic and static characteristics of the carotid sinus baroreflex in rats with chronic heart failure after myocardial infarction

Toru Kawada · Meihua Li · Atsunori Kamiya · Shuji Shimizu · Kazunori Uemura · Hiromi Yamamoto · Masaru Sugimachi

Received: 24 January 2010 / Accepted: 5 May 2010 / Published online: 1 June 2010

Abstract We estimated open-loop dynamic characteristics of the carotid sinus baroreflex in normal control rats and chronic heart failure (CHF) rats after myocardial infarction. First, the neural arc transfer function from carotid sinus pressure to splanchnic sympathetic nerve activity (SNA) and its corresponding step response were examined. Although the steady-state response was attenuated in CHF, the negative peak response and the time to peak did not change significantly, suggesting preserved neural arc dynamic characteristics. Next, the peripheral arc transfer function from SNA to arterial pressure (AP) and its corresponding step response were examined. The steady-state response and the initial slope were reduced in CHF, suggesting impaired end-organ responses. In a simulation study based on the dynamic and static characteristics, the percent recovery of AP was reduced progressively as the size of disturbance increased in CHF, suggesting that a reserve for AP buffering is lost in CHF despite relatively maintained baseline AP.

T. Kawada (✉) · M. Li · A. Kamiya · S. Shimizu · K. Uemura · M. Sugimachi
Department of Cardiovascular Dynamics, National Cerebral and Cardiovascular Center Research Institute, 5-7-1 Fujishirodai, Suita, Osaka 565-8565, Japan
e-mail: torukawa@res.ncvc.go.jp

M. Li · S. Shimizu
Japan Association for the Advancement of Medical Equipment, Tokyo 113-0033, Japan

H. Yamamoto
Division of Cardiology, Department of Internal Medicine, Kinki University School of Medicine, Osaka 589-8511, Japan

Keywords Systems analysis · Transfer function · White noise · Sympathetic nerve activity · Arterial pressure · Equilibrium diagram

Introduction

The arterial baroreflex is an important negative feedback system that stabilizes systemic arterial pressure (AP) against exogenous disturbances. The rapidness of AP regulation may be best described by the system dynamic characteristics. With respect to the sympathetic arterial baroreflex system, previous studies in rabbits [1] and rats [2] have indicated that the transfer function of the baroreflex neural arc from baroreceptor pressure input to efferent sympathetic nerve activity (SNA) exhibits "derivative" characteristics, which means that the dynamic gain of the SNA response to pressure perturbation becomes greater as the modulation frequency increases. On the other hand, the transfer function of the baroreflex peripheral arc from SNA to AP shows "low-pass" characteristics, which means that the dynamic gain of the AP response to SNA variation becomes smaller as the modulation frequency increases. In short, the neural arc provides an accelerating mechanism of the dynamic AP response in the arterial baroreflex system [1].

Although a number of studies have indicated that the baroreflex function is depressed in heart failure [3–6], dynamic characteristics of the arterial baroreflex in heart failure have not been fully described. The aim of the present study was to identify the open-loop dynamic characteristics of the carotid sinus baroreflex in a rat model of chronic heart failure (CHF) after myocardial infarction. To obtain a total picture of the AP regulation in CHF, we also estimated the open-loop static characteristics of the carotid sinus baroreflex.

Materials and methods

Animals were cared for in strict accordance with the Guiding Principles for the Care and Use of Animals in the Field of Physiological Sciences, which has been approved by the Physiological Society of Japan. All experimental protocols were reviewed and approved by the Animal Subjects Committee at the National Cerebral and Cardiovascular Center.

Myocardial infarction

Coronary artery ligation was performed under sterile conditions in 8-week-old male Sprague-Dawley rats according to a previously established procedure [7]. After inducing anesthesia by halothane inhalation, the rat was intubated and mechanically ventilated. The left chest was opened at the fourth intercostal space and the left coronary artery was ligated with a 5-0 polypropylene suture (PROLENE, Ethicon, GA, USA). An electrocardiogram was monitored for 1 h after the coronary ligation, and the heart was defibrillated as necessary by manual prodding. Thereafter air was evacuated from the thoracic cavity and the incision was closed. The rats were allowed to recover from anesthesia, and were fed ad libitum with a standard laboratory chow and given free access to water. Although we initially planned to wait until the rats showed an objective sign of advanced heart failure such as facial edema or labored breathing, the rats with such severe heart failure were too weak to survive the acute baroreflex study described in the following section. Accordingly, the rats that survived for 100–200 days (156 ± 18 days) after myocardial infarction were used without solid criteria for starting the acute baroreflex study. Instead, the rats were regarded as experiencing CHF when the central venous pressure was higher than 2.5 mmHg or the biventricular weight was greater than 2.5 g/kg body weight at the time of the acute baroreflex study.

Acute baroreflex study

Experiments were performed in normal control ($n = 12$) and CHF ($n = 7$) rats. Sham operation was not performed in the control rats. Among the control rats, eight rats were matched with the CHF rats based on body weight, but they were younger in age due to the retardation of growth in the CHF rats. The remaining four rats were age-matched with the CHF rats, but they were heavier in body weight. Because none of the parameters of the baroreflex dynamic and static characteristics differed statistically between the two subgroups of the control rats, we report pooled data obtained from the 12 control rats.

Each rat was anesthetized with an intraperitoneal injection (2 ml/kg) of a mixture of urethane (250 mg/ml) and α-chloralose (40 mg/ml), and mechanically ventilated with oxygen-enriched room air. A venous catheter was inserted into the right femoral vein, and 20-fold diluted anesthetic mixture was administered continuously (2–3 ml kg^{-1} h^{-1}). An arterial catheter was inserted into the right femoral artery to measure AP. Heart rate (HR) was obtained from AP through a cardiotachometer. Another venous catheter was inserted into the left femoral vein and advanced into the inferior vena cava to measure central venous pressure and to supply Ringer solution (6 ml kg^{-1} h^{-1}).

A postganglionic branch from the splanchnic sympathetic nerve was exposed through a left flank incision, and a pair of stainless steel wire electrodes (Bioflex wire AS633, Cooner Wire, CA, USA) was attached to record SNA. The nerve and electrodes were covered with silicone glue (Kwik-Sil, World Precision Instruments, FL, USA) for insulation and fixation. To quantify the nerve activity, the preamplified nerve signal was band-pass filtered at 150–1,000 Hz, and then full-wave rectified and low-pass filtered with a cut-off frequency of 30 Hz. Pancuronium bromide (0.4 mg kg^{-1} h^{-1}) was administered to prevent muscular activity from contaminating the SNA recording. At the end of the experiment, we confirmed the disappearance of SNA in response to an intravenous bolus injection of a ganglionic blocker, hexamethonium bromide (60 mg kg^{-1}), and recorded the noise level.

Bilateral vagal and aortic depressor nerves were sectioned at the neck to avoid reflexes from the cardiopulmonary region and aortic arch. The carotid sinus regions were isolated from the systemic circulation bilaterally according to previously reported procedures [8, 9]. Briefly, a 7-0 polypropylene suture with a fine needle (PROLENE, Ethicon, GA, USA) was passed through the tissue between the external and internal carotid arteries, and the external carotid artery was ligated close to the carotid bifurcation. The internal carotid artery was embolized using two to three steel balls (0.8 mm in diameter, Tsubaki Nakashima, Nara, Japan) injected from the common carotid artery. Under these conditions, the brain stem area was perfused by patent bilateral vertebral arteries. The isolated carotid sinuses were filled with warmed Ringer solution through catheters inserted into the common carotid arteries. Carotid sinus pressure (CSP) was controlled using a servo-controlled piston pump. Heparin sodium (100 U kg^{-1}) was given intravenously to prevent blood coagulation. Body temperature was maintained at approximately 38°C with a heating pad.

Protocols

After the above surgical procedures were completed, reflex responses in SNA, AP, and HR to CSP input were

monitored for more than 30 min. The rat was excluded from further study and analysis in the event that the reflex responses became smaller within this period. Possible causes for the deterioration in the reflex responses include surgical damage to the carotid sinus nerves and brain ischemia due to the bilateral carotid occlusion.

To estimate the dynamic input-output relationship of the carotid sinus baroreflex, CSP was perturbed for 20 min using a Gaussian white noise (GWN) signal with the mean of 120 mmHg and standard deviation of 20 mmHg. The selection of the mean pressure and amplitude of GWN does not significantly affect the estimation of the system dynamic characteristics except for a factor of proportionality (see Appendix 1 for details). The switching interval of GWN was set at 500 ms. The input power spectral density was relatively constant up to 1 Hz, which covered the upper frequency range of interest with respect to the sympathetic arterial baroreflex in rats [2].

To estimate the static input-output relationship of the carotid sinus baroreflex, CSP was decreased to 60 mmHg for 4–6 min, and then increased stepwise from 60 to 180 mmHg in increments of 20 mmHg every minute [10].

Data analysis

Data were sampled at 200 Hz using a 16-bit analog-to-digital converter and stored on a dedicated laboratory computer system. In each rat, the noise level of SNA recorded after the administration of hexamethonium bromide was treated as zero. Because the absolute voltage of SNA varied among animals depending on the recording conditions, SNA averaged during the last 10 s at CSP of 60 mmHg in the stepwise input protocol was defined as 100%. The same normalization factor was used for the analysis of the baroreflex dynamic characteristics.

Dynamic characteristics of the baroreflex neural arc, peripheral arc, total baroreflex, and HR control were estimated by an open-loop transfer function analysis as follows [11]. Data were analyzed from 90 s after the initiation of the GWN input. The input-output data pairs were resampled at 10 Hz and segmented into 50% overlapping bins of 1,024 points each. For each segment, a linear trend was removed, and a Hanning window was applied. Fast Fourier transform was performed to obtain the frequency spectra of the input and output signals. The ensemble averages of the input power spectral density [$S_{XX}(f)$], output power spectral density [$S_{YY}(f)$], and cross spectral density between the input and output signals [$S_{YX}(f)$] were calculated over 12 segments, where f denotes frequency. Finally, the transfer function [$H(f)$] from input to output was estimated as:

$$H(f) = \frac{S_{YX}(f)}{S_{XX}(f)} \tag{1}$$

The transfer function is a complex-valued function that can be expressed by the modulus and phase at each frequency. In the present study, we refer to the modulus of the transfer function as the dynamic gain. To quantify the linear dependence between the input and output signals, a magnitude squared coherence function [Coh(f)] was calculated as:

$$\mathrm{Coh}(f) = \frac{|S_{YX}(f)|^2}{S_{XX}(f)S_{YY}(f)} \tag{2}$$

The coherence function is a real-valued function ranging from zero to unity. When the output signal is perfectly explained by the linear dynamics with the input signal, the coherence value becomes unity. When the output signal is totally independent of the input signal, the coherence value becomes zero.

To facilitate understanding of the transfer function, the step response was also calculated as follows. The system impulse response was derived from the inverse Fourier transform of $H(f)$. The step response was then obtained from the time integral of the impulse response.

To quantify the open-loop static characteristics of the carotid sinus baroreflex, mean SNA, AP, and HR were obtained during the last 10 s at each CSP level of the stepwise input protocol. In each rat, data from two consecutive step cycles were averaged. The static characteristics of the baroreflex neural arc (the CSP-SNA relationship), the total baroreflex (the CSP-AP relationship), and the HR control (the CSP-HR relationship) were described by fitting four-parameter logistic functions to the input-output data as follows [10, 12]:

$$y = \frac{P_1}{1 + \exp[P_2(x - P_3)]} + P_4 \tag{3}$$

where x and y denote the input (CSP) and output (SNA, AP, or HR), respectively; P_1 is the response range of output; P_2 is the slope coefficient; P_3 is the midpoint pressure of input; and P_4 is the minimum value of output. For convenience, the maximum slope or the maximum gain of the logistic function is reported by a positive value as $P_1P_2/4$.

The static characteristics of the baroreflex peripheral arc (the SNA-AP relationship) were quantified by a linear regression analysis as follows [10, 13]:

$$\mathrm{AP} = a \times \mathrm{SNA} + b \tag{4}$$

where a and b represent the slope and intercept, respectively, of the regression line.

Statistical analysis

All data are presented in mean and SE values. Unpaired t tests were used to compare the parameters of the baroreflex dynamic and static characteristics between the control and CHF groups [13]. To compare the transfer functions between the two groups, we arbitrarily selected the dynamic gain values at 0.01, 0.1, and 1 Hz ($G_{0.01}$, $G_{0.1}$, and G_1). For the step response relating to the neural arc transfer function, the negative peak response (S_{peak}), the time to the negative peak (T_{peak}), the value of the step response at 10 s (S_{10}), the steady-state response at 50 s (S_{50}), and the ratio of the peak response to the steady-state response (S_{peak}/S_{50}) were calculated. For the step response relating to the peripheral arc, total baroreflex, or HR control, an initial slope of the response was calculated (see Appendix 2) in addition to S_{50}. Differences were considered significant when $P < 0.05$.

Simulation study

Once the open-loop dynamic and static characteristics of a system are both identified, closed-loop system responses can be simulated [14–16]. To compare closed-loop behavior of the carotid sinus baroreflex between control and CHF conditions, step inputs ranging from −10 to −60 mmHg were applied as exogenous disturbances, and resulting AP responses were simulated. Percent recovery was calculated as the magnitude of steady-state AP recovery relative to the size of step disturbance. The initial slope for the recovery response was also calculated (see Appendix 2).

Results

Postmortem examination confirmed that the left ventricular free wall was reduced to a membrane-like scar in the CHF group. Biventricular weights, both absolute and relative to body weight, were significantly greater in the CHF than in the control group (Table 1). The central venous pressure was significantly higher and the baseline AP and HR were significantly lower in the CHF group. Although the duration after myocardial infarction ranged from 100 to 200 days in the CHF group, there was no significant correlation between the duration and biventricular weight ($y = 0.0012x + 2.53$, $r^2 = 0.035$, $P = 0.72$, x duration in days, y biventricular weight in grams per kilogram) or between the duration and central venous pressure ($y = -0.013x + 7.5$, $r^2 = 0.07$, $P = 0.58$, x duration in days, y central venous pressure in millmeters of mercury).

Typical experimental recordings obtained from a control rat are shown in Fig. 1a. m-SNA indicates a 2-s moving averaged signal of SNA. In the dynamic input protocol, CSP was changed dynamically according to a GWN signal. m-SNA varied dynamically in response to the CSP perturbation. Although AP changed dynamically, the AP variation seemed more sluggish than the SNA variation. Changes in HR were less obvious from the time series data. In the static input protocol, a stepwise increase in CSP decreased m-SNA, AP, and HR. The noise level of SNA obtained after the intravenous administration of hexamethonium bromide was set at zero. Because of the normalization procedure, m-SNA during the last 10 s at CSP of 60 mmHg approximated 100%. Figure 1b represents CSP and SNA signals sampled at 200 Hz during the dynamic input protocol. High CSP inputs suppressed SNA to a noise level.

Typical experimental recordings obtained from a CHF rat are shown in Fig. 2a. In the dynamic input protocol, CSP was changed dynamically according to a GWN signal. Although m-SNA varied dynamically in response to the CSP perturbation, changes in AP and HR were not obvious from the time series data. In the static input protocol, a stepwise increase in CSP decreased m-SNA, AP, and HR. The magnitudes of the responses in m-SNA, AP, and HR seem smaller than those in the control rat. Figure 2b represents CSP and SNA signals sampled at 200 Hz during the dynamic input protocol. High CSP inputs suppressed SNA to a noise level.

Dynamic characteristics of the carotid sinus baroreflex

Figure 3 summarizes the open-loop dynamic characteristics of the carotid sinus baroreflex averaged for the control

Table 1 Age, body weight, biventricular weight, central venous pressure, mean arterial pressure, and heart rate of the normal control and chronic heart failure (CHF) rats

Data are presented as mean ± SE

** $P < 0.01$ and * $P < 0.05$ by unpaired t test

	Control (n = 12)	CHF (n = 7)	P value
Age at experiment (weeks)	24 ± 3	30 ± 3	0.237
Body weight (g)	565 ± 28	538 ± 19	0.474
Biventricular weight (g)	1.16 ± 0.04	1.45 ± 0.08**	0.002
Biventricular weight (g kg body weight^{-1})	2.05 ± 0.06	2.71 ± 0.13**	<0.001
Central venous pressure (mmHg)	2.0 ± 0.2	5.4 ± 0.9**	<0.001
Mean arterial pressure (mmHg)	134 ± 4	121 ± 4*	0.037
Heart rate (beats min^{-1})	414 ± 11	350 ± 12**	0.001